Journal of Hydrology 556 (2018) 449–474

Contents lists available at ScienceDirect

Journal of Hydrology

journal homepage: www.elsevier.com/locate/jhydrol

Research papers

Insights on pumping well interpretation from flow dimension analysis: The learnings of a multi-context field database

Anouck Ferroud *, Romain Chesnaux, Silvain Rafini

Research Group R2Eau, Centre d'études sur les ressources minérals, Université du Québec à Chicoutimi, 555 boulevard de l'Université, Chicoutimi, Québec G7H 2B1, Canada

ARTICLE INFO

Article history:
Received 23 December 2016
Received in revised form 26 September 2017
Accepted 4 October 2017
Available online 7 October 2017
This manuscript was handled by Peter K. Kitanidis, Editor-in-Chief, with the assistance of Adrian Deane Werner, Associate Editor

Keywords:
Diagnostic plot
Drawdown log-derivative signal
Flow dimension
Theis-derived models
Complex aquifers
Field data

ABSTRACT

The flow dimension parameter n, derived from the Generalized Radial Flow model, is a valuable tool to investigate the actual flow regimes that really occur during a pumping test rather than suppose them to be radial, as postulated by the Theis-derived models. A numerical approach has shown that, when the flow dimension is not radial, using the derivative analysis rather than the conventional Theis and Cooper-Jacob methods helps to estimate much more accurately the hydraulic conductivity of the aquifer. Although n has been analysed in numerous studies including field-based studies, there is a striking lack of knowledge about its occurrence in nature and how it may be related to the hydrogeological setting. This study provides an overview of the occurrence of n in natural aquifers located in various geological contexts including crystalline rock, carbonate rock and granular aquifers. A comprehensive database is compiled from governmental and industrial sources, based on 69 constant-rate pumping tests. By means of a sequential analysis approach, we systematically performed a flow dimension analysis in which straight segments on drawdown-log derivative time series are interpreted as successive, specific and independent flow regimes. To reduce the uncertainties inherent in the identification of n sequences, we used the proprietary SIREN code to execute a dual simultaneous fit on both the drawdown and the drawdown-log derivative signals. Using the stated database, we investigate the frequency with which the radial and non-radial flow regimes occur in fractured rock and granular aquifers, and also provide outcomes that indicate the lack of applicability of Theis-derived models in representing nature. The results also emphasize the complexity of hydraulic signatures observed in nature by pointing out n sequential signals and non-integer n values that are frequently observed in the database.

1. Introduction

The discrepancy between the complexity of real flow behavior and the simplicity of analytical flow models makes the interpretation of transient well tests an ambiguous and imprecise task. Hydrogeology practitioners routinely interpret constant-rate pumping tests by matching theoretical type-curves obtained from Theis-derived models, thus ignoring the real flow regime that occurs during the test and neglecting the idealized Theis assumptions that suppose a totally penetrating well, the homogeneity of the aquifer and the infinite acting radial flow. This matching procedure, or "fit", requires the practitioner to make the implicit postulate that the flow regime is cylindrical-radial. The term "flow regime" refers here to the pressure behavior and does not relate to any laminar or turbulent flow regimes, as defined by the Reynold number. While cylindrical-radial flow is a common pumping test response, the careful examination of well test results from a variety of geologic environments reveals that other, non-cylindrical-radial flows are also common and that they may change over the course of a well test. Theis-derived models are only valid for cylindrical-radial flow. Their application to systems with non-cylindrical-radial behaviors may lead to a significant degree of error, leading to a poor understanding of the hydrodynamic behavior of the aquifer and requiring a substantial degree of approximation when estimating the aquifer's hydraulic properties. As stated by Le Borgne et al. (2004), the estimation of the transmissivity T and the storage coefficient S depend directly on the flow dimension value as $T = b^{3-n}.K$ and $S = b^{3-n}.S_s$. This paper uses an extensive database of both fractured and non-fractured environments to show that non-cylindrical-radial flow regimes are widespread, and must be considered in the analysis of well test data.

One of the fundamental issues in hydrogeology is the capability of estimating aquifer's hydraulic parameters in a more representative and accurate manner. For instance, hydraulic conductivity (K) is an essential parameter used to characterize groundwater flow

* Corresponding author.
E-mail address: anouck.ferroud1@uqac.ca (A. Ferroud).

https://doi.org/10.1016/j.jhydrol.2017.10.008
0022-1694/

fields, predict contaminant transport (Carrera, 1993; Rozemeijer et al., 2010; Barlow and Coupe, 2012) and delineate wellhead protection areas (WHPA) (Bear and Jacobs, 1965; Wyssling, 1979; Todd, 1980; Grubb, 1993). It is essential to reduce the degree of uncertainty of K because this value controls the size, shape and location of wellhead capture zones (Bhatt, 1993; Forster, et al., 1997; Fadlelmawla and Dawoud, 2006; Paradis et al., 2007; Barry et al., 2009).

In 1989 in the petroleum literature, Bourdet et al. proposed that in addition to plotting the pressure data p, practitioners and modellers should also plot the pressure derivative signal $dp/dlogt$. This is easily implemented in hydrogeology in the form of the drawdown log-derivative signal $ds/dlogt$ (Renard et al., 2009). Rather than using a simple drawdown signal s, the derivative approach makes the signal much more sensitive to small variations of drawdown. The diagnostic plots, representing the combined plots of both s and $ds/dlogt$ *versus* time, are thus used in particular to improve the interpretation of constant-rate pumping tests. Two different methods can be employed to interpret this derivative signal: matching type curves over the entire signal or decomposing the signal into straight lines. In the first method, an analytical flow model is selected and its theoretical curve is matched to the derivative data. The match is generally performed using automatic best-fitting codes (Leveinen et al., 1998; Kuusela-Lahtinen et al., 2003; Verbovšek, 2009). To select the analytical model that most suitably represents the real flow regime, $ds/dlogt$ is considered. The second method is a straight-line analysis that consists in decomposing the hydraulic signal into straight lines that are interpreted separately from each other in terms of their hydrodynamic behavior. Usually plotted on a log-log scale, the diagnostic plots make it possible to better take into consideration the heterogeneity of aquifers. Using this sequential approach of flow regimes, the hydraulic properties of the aquifer can be estimated according to the TDS (Tiab's Direct Synthesis) philosophy (Tiab 1994, 1995). This approach, chiefly used in the petroleum literature, establishes equations based on the intersections points and slopes of the $ds/dlogt$ straight lines to estimate the parameters of the well and of the aquifer that control the flow regime. Petroleum researchers developed equations for specific conceptual models established in view of determining parameters such as: permeability, skin factor, wellbore storage coefficient, hydraulic conductivity of fractures, half-fracture length and drainage area (Tiab, 2005; Escobar et al., 2007; Escobar et al., 2010, Escobar et al., 2012).

The flow dimension is a parameter proposed by Barker in 1988. It expresses the evolution of the shape of the pressure-front pulse as it diffuses through the aquifer during the transient stage of pumping. The flow dimension identifies, by a value $n = 2$, the occurrence of a cylindrical-radial flow regime during the pumping test, associated with a zero slope of $ds/dlogt$ when plotted on the log-log axis. The non-cylindrical-radial flow dimensions are easily recognised when $ds/dlogt$ displays a rising straight line (positive slope) for $n < 2$, and a declining straight line (negative slope) for $n > 2$. The interpretation of pumping tests, supposing cylindrical-radial flow, is thus performed more accurately and swiftly by easily detecting when the Theis-derived assumptions are suitable. This better compliance with assumed and real flow geometries may reduce uncertainties in the determination of hydraulic properties. As stated by Black (1994), if the flow dimension is assumed to be 2 while in fact it is closer to 1, the hydraulic diffusivity will be underestimated. Furthermore, for the specific case of $n = 2$, K is directly estimated from the y-axis intercept of $ds/dlogt$ on log-log scales (Barker, 1988). For cases where a vertical fault produces a bilinear flow regime ($n = 1.5$), Rafini and Larocque (2009, 2012) developed an equation that makes it possible to estimate K graphically, without type-curve matching. The most significant advantage of the flow dimension lies in the fact that it provides a relationship between the drawdown log-derivative signal and the flow regime occurring during the pumping test, for any hydrodynamic circumstance (cylindrical-radial and non-cylindrical-radial flow regimes). The $ds/dlogt$ approach significantly improves the transient test interpretation method because makes it possible to investigate the flow regimes detected by the transient test, instead of assuming them. Despite its diagnostic potential for interpreting transient well tests, the n parameter is still seldom used, due to the difficulty of relating the flow dimension values to conceptual aquifer conditions such as flow patterns and geological settings. So far, only a few values of n have been assigned a physical interpretation, and thus its diagnostic potential remains only partially exploited.

Advances in the conceptual understanding of n have been achieved though several numerical modelling studies. These studies concentrate on the influence exerted by various configurations or mechanisms on the $ds/dlogt$ signal. We may mention research works that have focused on: the geometry of the boundaries (Beauheim and Roberts, 1998; Walker and Roberts, 2003; Escobar et al., 2005, 2007), the wellbore effects (Jourde et al., 2002b; Escobar et al., 2012), the properties of fractured rock (Jourde et al., 2002a; Cello et al., 2009) and the properties of faults (Gringarten et al., 1974; Cinco-Ley et al., 1978; Abbaszadeh and Cinco-Ley, 1995; Rafini and Larocque 2009, 2012). These studies contributed to the evolution of the physical conceptualization of flow regimes. They proposed specific conceptual models to interpret the flow geometry, the configuration of the hydraulic properties and the boundary conditions of a specific flow regime sequence.

In the literature, the flow dimension parameter is sporadically used to characterize the hydraulic properties of aquifers (Leveinen et al., 1998; Liang et al., 2012). Only a few studies have described the frequency of occurrence of n in nature: one in dolomite (Verbovšek, 2009, 2011), one in fractured limestone (Audouin and Bodin, 2008), one in fractured crystalline rock (Kuusela-Lahtinen et al., 2003) and one in weathered crystalline rock (Maréchal et al., 2004). Other studies have provided specific case study analyses: one in granitic and carbonate rocks (Bangoy et al., 1992), one in poorly-weathered crystalline rock (Leveinen, 2000), sixteen in evaporite deposits (Beauheim and Roberts, 2002) and five in fractured rock aquifers (Lods and Gouze, 2004).

These studies showed that the majority of n values lie within a range of 1–3 and that the radial flow dimension is seldom observed (Table 4). The authors (Kuusela-Lahtinen et al., 2003; Audouin and Bodin, 2008; Verbovšek, 2009) each analyzed only one geological family. They limited themselves to correlating the distribution of n with the geology, but did not propose a hypothesis regarding the conceptual model or the geological facies that provide the water supply and control the flow regimes. Furthermore, the majority of the wells analyzed in these studies belong to the same aquifer. The observations and conclusions of these studies should be examined by comparing aquifers in various locations.

This article proposes to open novel perspectives as it examines the distribution of n in various geological environments in nature. We examine constant-rate pumping tests (lasting 3.1 days on average) performed in various aquifers composed of fluvio-glacial deposits, crystalline and carbonate rocks. This study has two main objectives: i) to survey the suitability of Theis and Theis-derived model assumptions for reproducing flow dimensional behaviors in natural aquifers, ii) to provide objective and comprehensive records of occurrences of natural flow dimension, with insights on the relationships between n and the features of various different aquifers. Over the last three decades, flow dimensions have been subjectively reported in the literature in the context of introductions of published articles describing specific interpretative models. The real distribution of flow dimension values in various types of natural media have remained undocumented, even though

flow dimension undoubtedly constitutes a key and reliable indicator of the physical attributes of an aquifer. Comparing flow dimension distribution patterns against their associated geological frameworks will provide insights about their possible conceptual interpretation. This study is the first to attempt to perform a statistical analysis of the flow dimensions observed in nature, based on a sequential derivative analysis, and to provide an initial portrait of the flow dimension distribution in both fractured rock aquifers and fluvio-glacial deposits. In an *n*-sequential analysis, the log-log plot of the drawdown log-derivative signal is considered a diagnostic tool. It is used to help interpret the flow geometry, the aquifer geometry and the heterogeneity of hydraulic properties, all there of which are detected as the pressure font pulse expands through the aquifer. We will firstly review the basic concepts of the GRF model, and then propose a reinterpretation of transient pumping tests conducted in wells. To this end we will use a database derived from 69 constant-rate pumping tests (lasting 3.1 days on average) conducted in the framework of consulting projects for municipal groundwater supplies in the Province of Quebec, Canada, in France and in Tunisia. A flow-dimension-sequence diagnostic approach is adopted for this reinterpretation of pumping tests, meaning that each slope of the drawdown log-derivative signal is interpreted as a specific and independent flow regime. Such analysis may be efficiently performed using the proprietary SIREN code, specifically designed to routinely interpret flow dimension sequences by simultaneously fitting drawdown and drawdown log-derivative data, respectively, on semi-log and log-log plots. This approach combines the advantages of both plots: the former is weakly influenced by pumping rate changes but grossly insensitive to flow regime, the latter is highly sensitive to flow regime changes but subject to strong noise effects due, for instance, to pumping rate instabilities. This study aims at contributing to our understanding of the physical interpretation of *n* through a statistical analysis of its natural occurrences in various geological media and by comparing the hydrodynamic interpretation of *n* against the conceptual models of the geology surrounding the wells. Finally, some ideas will be discussed regarding current practices in hydrogeology and the diagnostic potential of an approach which combines conventional plots, drawdown log-derivative plots and flow dimension analysis. While an extensive review of interpretative models using log-derivative analysis is beyond the scope of this paper, existing flow regime sequences will be investigated in detail and compared to the theoretical and geological conceptual models.

2. Theory and practice

2.1. Conventional analysis

The Theis model (1935) describes a transient cylindrical-radial flow, induced by a constant-rate pumping test within a confined, homogeneous, isotropic, horizontal-slab, totally screened and laterally infinite aquifer. In such conditions, also called Infinite Acting Radial Flow (IARF) conditions, the pressure front diffuses radially in the form of concentric circles (Fig. 1). The pressure front pulse generates an equipotential cross-flow surface *A(r)* which grows radially in the shape of a cylinder (Fig. 1), producing the ideal cylindrical-radial flow conditions referred to as Theis aquifers. A distinction must be made between the Theis model and the concept of radial flow regime, which strictly describes the proportional relationship between the cross-flow surface *A* and the travelled distance *r* from the pumping well, regardless of the shape of this surface. Most analytical solutions published during the three last decades in the petroleum literature, and classically used in the diagnostic plot approach (Bourdet et al., 1983; Renard et al., 2009), account for some variations on the cylindrical-radial flow theme, including either its combination with some external sources (unconfined aquifers; leaky aquifers as described by Hantush, 1956, 1960), some specific overlaying of several Theis aquifers (dual-porosity models; leaky aquifers as described by Neuman and Witherspoon, 1969). These models actually describe various types of radial flow regimes, which in itself does not signify that the flow geometry they are modelling remains ideally cylindrical-radial. In this study, these models will hereafter be referred to as Theis-derived models.

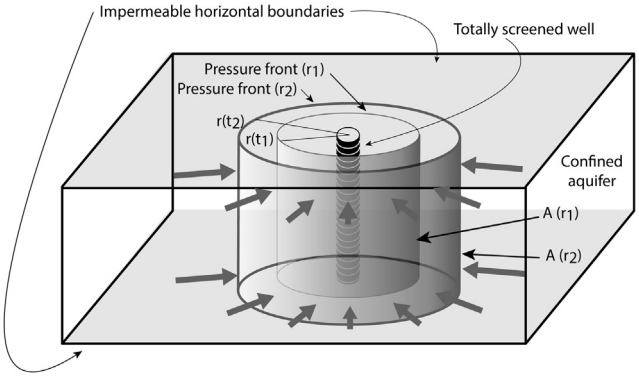

Fig. 1. Conceptual Theis model (1935) representing its main assumptions. The thick arrows represent the flow induced by the pumping test. In these IARF conditions, the cross-flow area *A(r)* extends radially in the form of cylinders and the pressure front pulse expands radially in the form of concentric circles having a radius *r(t)*. This flow behavior is called the cylindrical-radial flow regime.

In a system characterized by a diffuse short-scale field of heterogeneities, *T* and *S* may be averaged over the cross-flow area *A(r)*, making it possible to estimate the properties of the aquifer as being continuous and homogeneous. When the pressure front pulse reaches a large-scale heterogeneity within the aquifer, its shape may be deformed, leading to modifications in the equipotential surface growth pattern. The cylindrical-radial flow regime assumption can no longer be applied, rendering any Theis-derived model irrelevant.

Numerical modelling by Meier et al. (1998) and Sánchez-Vila et al. (1999) showed that for late-time drawdown and under cylindrical-radial flow conditions, the Cooper-Jacob approximation allows a good approximation of transmissivity but an erroneous estimation of storage coefficient in systems with a diffuse heterogeneity field and a radially convergent flow (Meier et al., 1998; Pechstein et al., 2016). These studies validated the applicability of the Cooper-Jacob model in specific heterogeneous domains with diffuse transmissivity fields and a concentric heterogeneous storage, conditions that allow the establishment of a cylindrical-radial flow regime. Meier et al. (1998) concluded their study by explaining that further numerical studies with three-dimensional flow conditions are needed to analyze flow behavior in aquifers with variable thicknesses. Cases of an increasing aquifer thickness (Dal Soglio, 2012; Rafini et al., 2014) or a partially screened or a partially penetrated aquifer (Moncada et al., 2005; Escobar et al., 2012; Ferroud et al., 2015) have been numerically documented to produce spherical flow regimes. In these non-cylindrical-radial conditions, Theis-derived approaches are undoubtedly unsuitable.

2.2. The Generalized Radial Flow model

2.2.1. Basic concepts

The Generalized Radial Flow (GRF) model was proposed by Barker in 1988, in response to the inability of conventional models to reproduce the flow within the fractured aquifer of Stripa mine

(Barker, 1988). The concept of the GRF model is based on a proportional relationship between A [L^2], the cross-flow area and r^{n-1}, the radial distance from the borehole of the pressure front pulse to the power of the flow dimension minus one (Eq. (1)):

$$A(r) \sim r^{n-1} \tag{1}$$

The parameter n is a value "that must be determined empirically and which may not have an integer value" (Barker, 2007). n reflects the rate by which the cross-flow area changes as a function of the distance from the well. As the pressure front pulse extends outwards and reaches heterogeneities within the aquifer, it may be deformed in such a manner that Eq. (3) is modified, inducing changes in the flow dimension. The sequences of n thus reflect flow regime changes induced by some variations in the physical or hydraulic features in the aquifer. Short pumping tests, because they induce only a limited cross-flow area expansion in the aquifer, mainly reflect wellbore effects and a small proportion of the aquifer in the vicinity of the well. It is the long-term pumping tests that may more accurately reflect the aquifer signal sensu stricto and the influence of boundary conditions.

The term "flow regime" thus refers to the behavior of the pressure front pulse as it moves through the aquifer. It is worth noting that the sequential analysis we employ in this study is an extension of the GRF model, since Barker (1988) defined media with constant n values assuming homogeneous conditions. By verifying the validity of Barker's equation (Eq. (1)) in a non-uniform, faulted aquifer, Rafini and Larocque (2009, 2012) proved that n is a valuable tool for interpreting the successive flow regimes that occur during a medium- or long-term pumping test, even if the aquifer does not have GRF-like properties in accordance with Barker's postulates. Each value of n independently observed at different times during the pumping test represents the dominant flow regime felt at that time by the pressure front pulse as it diffuses throughout the aquifer around the well at a distance $r(t)$.

Using the *GRF* concept, Barker (1988) introduced the flow dimension n in the diffusivity equation. The generalized diffusivity equation is written as (Eq. (2)):

$$\frac{K}{r^{n-1}}\frac{\partial}{\partial r}\left(r^{n-1}\frac{\partial h}{\partial r}\right) = S_s\frac{\partial h}{\partial t} \tag{2}$$

where K [LT^{-1}] is the hydraulic conductivity, r [L] is the radial distance from the borehole at time t [T], n is the flow dimension, S_s [L^{-1}] is the specific storage and h [L] is the hydraulic head.

Based on Eq. (2), using the Laplace transform tables and supposing constant head boundaries, a zero initial head and a long time t or a short distance r, Barker predicts the hydraulic head distribution as (Eq. (3)):

$$h(r,t) = \frac{Q}{4\pi^{1-\nu}Kb^{3-n}\nu}\left[\left(\frac{4Kt}{S_s}\right)^{\nu} - \Gamma(1-\nu)r^{2\nu}\right]\nu\neq 0 \tag{3}$$

$$\nu = 1 - \frac{n}{2} \tag{4}$$

With b the extent of the flow zone [L] and Γ the gamma function. Note that Eq. (3) is the asymptotic form of GRF's general solution (valid for u small enough with $u = S_s r^2/4Kt$), which is an incomplete gamma function.

Eq. (3) can be rewritten with a time-dependent term Ct^{ν} and time-independent term C' as:

$$h(t) = Ct^{\nu} + C' \tag{5}$$

with

$$C = \frac{Q}{4\pi^{1-\nu}Kb^{3-n}\nu}\left(\frac{4K}{S_s}\right)^{\nu} \tag{6}$$

and

$$C' = \frac{-Q}{4\pi^{1-\nu}Kb^{3-n}\nu}\Gamma(1-\nu)r^{2\nu} \tag{7}$$

Deriving Eq. (5) with respect to time shows that the drawdown log-derivative $ds/dlogt$ time series (Eq. (8)) displayed on a log-log plot forms a straight line with slope ν, providing a mean of a straightforward graphic determination of the flow dimension using Eq. (4).

$$\frac{ds}{dlogt} = \frac{t}{2.3}\frac{ds}{dt} = \frac{C}{2.3}\nu t^{\nu} \tag{8}$$

From a practical standpoint, when interpreting drawdown time series at the pumping well, the asymptotic condition is reached very early and can be considered valid during the whole aquifer-related response beyond the early influence of the wellbore effects. Note that in the petroleum literature, this asymptotic flow behavior is also named «infinite acting behavior». According to Eqs. (4) and (8), the derivative signal depends on Q, K, S_s, b and n. Thus, any modification of these parameters will be felt by the derivative signal. Note that only changes of K and S_s will temporarily invalidate the asymptotic assumption of the derivative signal (Eq. (3) is valid when u is small enough). Yet, straight derivative segments represent a sufficient proof of the validation of the asymptotic assumption. Before the pressure front pulse reaches the hydraulic boundaries, each straight-line segment is associated with a n value and represents a flow period during which Q, K, S_s and b are constant and/or uniform. As stated by Beauheim et al. (2004) and Rafini et al. (2017), we suggest that the flow dimension should be estimated from a constant straight line of $ds/dlogt$ that lasts at least one log-cycle.

We favor this graphic approach (Eq. (8)) without type-curve matching because it allows us to decompose the signal in a sequence of successive flow regimes associated to specific geological facies and flow behaviors. Because n is directly determined from the $ds/dlogt$ straight line slopes, which implies that it can assume any integer and non-integer value, it is a valuable parameter for statistically analysing the flow regimes of natural aquifers.

2.2.2. Conceptual interpretation of n

The main known flow dimensions (interpreted using Eq. (1)) are briefly summarized in this section. For further details, the reader is invited to refer to the original papers.

$n = 0$ ($\nu = 1$)

Observed early in the pumping test, this unit slope line of the drawdown log-derivative refers to wellbore effects (skin and wellbore storage) (Tiab, 1993; Mattar, 1997). Observed late in the pumping test, this flow regime may express the attainment of a stagnant state ("pseudo-steady-state flow" as described by Mattar, 1997), achieved when all the outer boundaries are no-flow boundaries, i.e., when the reservoir depressurizes without spatial diffusion of drawdown.

$n = 1$ ($\nu = 0.5$)

The linear flow implies that the cross-flow area remains constant as the pressure wave travels through the aquifer. Such conditions are observed in long and narrow systems which may be found: i) in granular channelized aquifers (fluvial and deep sea fans) (Escobar et al., 2004a; Escobar and Montealegre-M, 2007; Escobar et al., 2010; Corbett et al., 2012); ii) in fractured media containing an infinite-conductivity vertical fault (Gringarten and Witherspoon, 1972; Gringarten et al., 1974), iii) in fractured rocks with a finite-conductivity one-dimensional conduit formed by the

intersection of fractures and iv) in karst systems (Maréchal et al., 2008). A linear flow can also be observed in a planar fracture with channeling or preferred flow paths (Tsang and Neretnieks, 1998).

$n = 2$ $(v = 0)$

The radial flow regime is observed when the cross-flow area grows proportionally to the radial distance r. Such a condition can be produced by a cylindrical-radial flow regime. This flow regime is generally associated with a homogeneous and isotropic aquifer of uniform thickness, but other conceptual models may produce a radial flow dimension. Heterogeneous media may also produce a radial flow regime, such as a well located close to a vertical fault, when the matrix supply masks the signature of the fault (Cinco-Ley et al., 1978; Rafini and Larocque, 2009) or an orthogonal discontinuity network (Jourde et al., 1998).

$n = 3$ $(v = -0.5)$

The spherical flow regime is observed when the cross-flow area expands proportionally to r^2. According to Eq. (4), a spherical flow dimension is represented by a −0.5 negative slope of $ds/dlogt$ which reflects a drawdown rate deceleration that may be observed early in the pumping test, when the screen is very short relative to the aquifer. For instance, a spherical flow regime can be induced by a point source (between packers), by a partially penetrating well, by a partially completed well or by a restricted producing interval (Culham, 1974; Moncada et al., 2005; Escobar et al., 2012; Ferroud et al., 2015).

$n = \text{non} - \text{integer}$

The fractional (non-integer) flow regimes, which are frequently exhibited by field data diagnostic plots, have long been interpreted as being related to the geometry of the source (Barker, 1988) or to the fractal properties of the fractured media (Barker, 1988; Polek et al., 1989; Chang and Yortsos, 1990; Bangoy et al., 1992; Acuna and Yortsos, 1995). By analysing fractured systems that are generated from a fractal model using a Discrete Fracture Network, other authors (Geier et al., 1996; Winberg, 2000; Cello et al., 2009) showed that there exists a relationship between the flow dimension parameter and the connectivity of fractures. Other authors (like Jourde et al., 1998) interpreted the fractional flow dimension to be related to the connectivity of fractures in an orthogonal fracture network in tabular stratified aquifers. In 1991, the interpretation of fractional flow dimensions was widened to involve new considerations. In fact, Doe (1991) opened the fractional flow dimension definition to non-fractal geometries which are not space-filling. In other words, Euclidian configurations, with heterogeneity either in conductivity or geometry or a combination of both, can produce non-integer values of n. Bowman et al. (2012) simulated the flow through high-transmissivity conduits characterized by non-radial and simple geometries. By means of the flow dimension concepts developed by Doe (1991), Bowman et al. (2012) showed that the variability of conduit shape can generate non-integer flow dimensions such as 0.8, 1.2 and 1.6. In addition, the bilinear flow regime ($n = 1.5$) has been reported to reflect the signal of a finite-conductive fault supplied by the matrix. Such a configuration has been demonstrated analytically by Abbaszadeh and Cinco-Ley (1995) and then corroborated numerically by Rafini and Larocque (2009). The karst systems are also known to generate fractional flow dimension values that generally range between 0 and 1 (Maréchal et al., 2008; Giese et al., 2017). Finally, Walker and Roberts (2003) suggested that the flow dimension depends on the form of the nonstationary transmissivity (for instance, an aquifer presenting an exponential variation of thickness).

3. Data and method

3.1. Compilation of a pumping-well test database

A database mainly composed of 69 pumping-well tests (with a mean duration of 3.1 days ranging from 0.2 to 14.7 days) and of local geological information has been established (Table 1). Most of the compiled data come from pumping-well tests conducted in the framework of municipal groundwater supply investigations in the province of Quebec (Canada) regions of Charlevoix-Haute-Côte-Nord (CHCN), Saguenay-Lac-Saint-Jean (SLSJ) (Chesnaux et al., 2011) and Abitibi-Temiscamingue (ABTE) (Nadeau et al., 2015). Additional data were obtained from i) south-eastern Quebec (Mirabel) (Nastev et al., 2004); ii) various locations in France (regions of the Alps, Midi-Pyrenées, Nord-Pas-de-Calais and Loire); iii) the database *Banque de données du sous-sol* compiled by the *Bureau de Recherches Géologiques et Minières* (BRGM) and iv) in northern Tunisia.

3.2. Data pre-processing

Log-derivative data are typically very noisy. This may be due to datalogger or operator complications, pumping rate variations, random diffuse heterogeneity fields and tidal or recharge effects. We therefore smooth the data using the algorithm of Bourdet et al. (1989) which has proven to be one of the most efficient in filtering noise without deteriorating the hydraulic signature (Escobar et al., 2004b). The differentiation equation is:

$$\frac{ds_i}{dX_i} = \frac{\left(\frac{\Delta s_1}{\Delta X_1}\Delta X_2 + \frac{\Delta s_2}{\Delta X_2}\Delta X_1\right)}{(\Delta X_1 + \Delta X_2)} \tag{9}$$

with: $\Delta s_1 = s_i - s_1$; $\Delta s_2 = s_i - s_2$; $\Delta X_1 = X_i - X_1$; $\Delta X_2 = X_i - X_2$ and $X = \log(t)$.

Eq. (9) uses 3 points: the next and previous points (1 and 2) of point i which are the first to be separated by a minimum length of L. The length can thus be adjusted until the noise is attenuated and the signal is no longer distorted.

The drawing of straight lines is performed manually by considering the differentiation curves for various L values (Eq. (9)). Furthermore, the simultaneous dual fits performed with SIREN are such that when derivative data are too noisy or disrupted, the drawdown fit makes it possible to attenuate the uncertainties inherent in the assessment of derivative linear regressions.

In order to quantify the quality of each manual fit, the coefficient of determination R^2 is calculated between the differentiated points and the regression line, defined manually.

Fig. 2-A displays the effects of pumping rate adjustments (at 55, 243 and 3390 min) on the s and $ds/dlogt$ responses. On the upper plot, s shows a slight translation of the signal for each of the three changes of pumping rate Q. The rate values are unfortunately not mentioned in the consultant's report but the increase of the drawdown signature suggests an increase of Q for each adjustment. On the lower plot, the $ds/dlogt$ signal shows a small number of extreme and noisy data when the pumping rate is increased but afterwards, the initial flow regime is rapidly recovered. The flow dimension value is thus not influenced by variations in the constant pumping rate.

Fig. 2-B shows the effects of an interruption in pump operation (between 3 and 4 min) on the s and $ds/dlogt$ responses. On the upper plot, s displays a reduction of drawdown associated with an increase of hydraulic head in the well, until the pump is restarted (approximately 10 min). Derivative data show a pseudo-spherical flow regime ($n = 2.6$), which is totally disrupted by the pump interruption. Indeed, between 3 and 10 min (Fig. 2-B), the pumping stops and induces a recovery of the signal

Table 1
Long-term pumping tests included in the pooled database: location of wells and observed lithology.

	Number of observations							Total %
	All sources	CHCN (Quebec)	SLSJ (Quebec)	Mirabel (Quebec)	ABTE (Quebec)	Tunisia	France	
Alluvial deposits	22	6	8	1	7	0	0	32 %
Crystalline rocks	19	9	2	2	0	0	6	28 %
Carbonates	28	2	1	14	0	2	9	41 %
Total	69	17	11	17	7	2	15	100 %

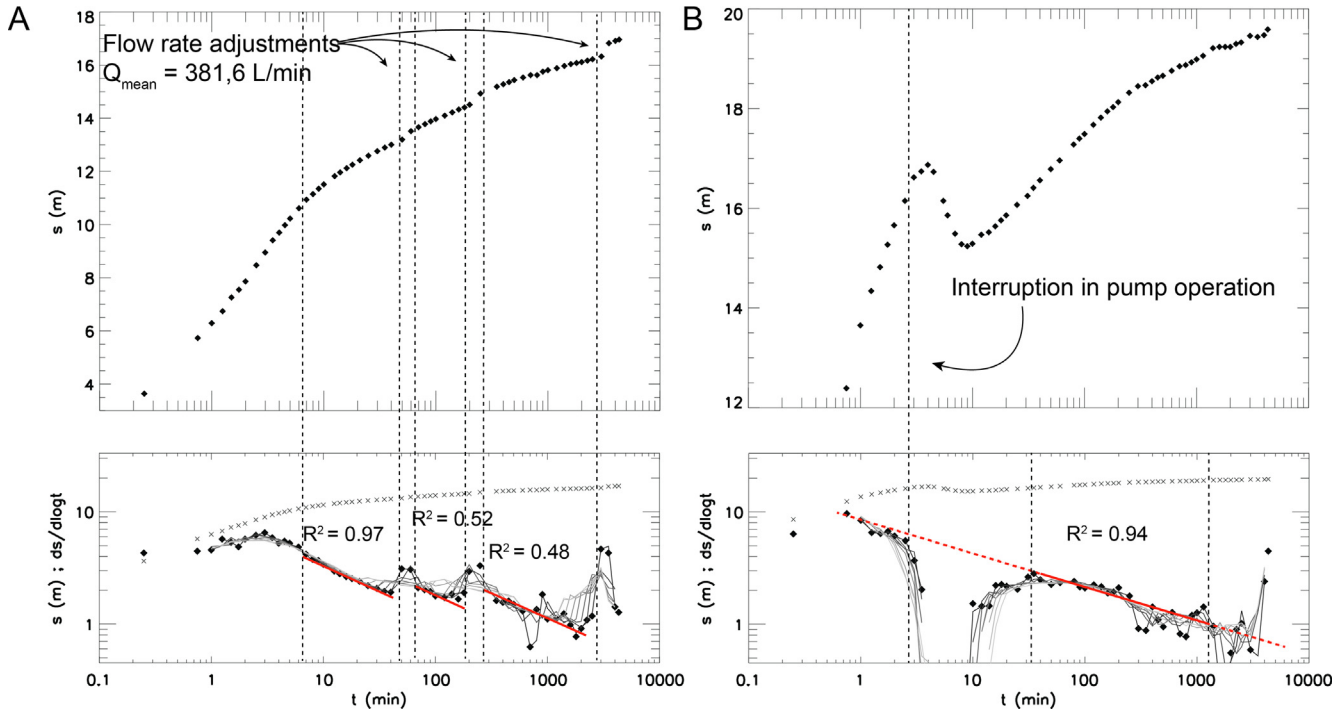

Fig. 2. Diagnostic plots of two pumping tests performed in two wells in alluvial deposits showing A) the effects of pumping rate adjustments and B) the effect of a temporary interruption of the pump on the *s* and *ds*/*dlogt* signals. The diamond shapes represent the drawdown log-derivative signal and the "x" shapes represent the drawdown signal. The grey lines, derived from the algorithm of Bourdet et al. (1989), represent seven data smoothings for *L* ranging between 0.2 and 0.8. The R^2 value represents the coefficient of determination between the derivative data and the regression line.

yielding negative data of the derivative which are not visible on a log-log plot. When the pump restarts, the general trend is rapidly recovered, with no evidence of pump disturbance (straight line in Fig. 2). In both case studies (Fig. 2-A and B), the derivative signal quickly returns to normal due to the high hydraulic conductivity of the alluvial deposit, which is estimated in the order of $3{,}5 \times 10^{-5}$ m/s. Note that this value is estimated from a conventional cylindrical-radial flow dimension model, and therefore, it is properly estimated in the case of an aquifer that instead induces a spherical flow dimension.

Numerical simulations were conducted in order to confirm these field observations and to clarify the flow regime behavior when the hydraulic test is affected by pumping rate changes or by a pump shut-down. The four columns of Fig. 3 show the drawdown and drawdown-log derivative signals of four different conceptual models, which are generated in confined conditions using the HydroGeoSphere code (Therrien et al., 2010). Each of the four conceptual models generates distinct flow dimension sequences. From left to right of Fig. 3, the *n*-sequences are: cylindrical-radial to linear (n = 2–1), bilinear to cylindrical-radial (n = 1.5–2), simply cylindrical-radial (n = 2) and spherical to cylindrical-radial (n = 3–2). The cylindrical-radial-linear *n*-sequence is obtained by generating a flow within a conduit. The bilinear to cylindrical-radial *n*-sequence is obtained by a well connected to a finite-conductive vertical fault supplied by the matrix. The cylindrical-radial flow regime is modeled with a conventional Theis aquifer. The spherical-radial *n*-sequence is induced by a well that partially penetrates the aquifer. From top to bottom, Fig. 3 shows the semi-log plot of the drawdown (CP_1, CP_2, CP_3 and CP_4), the drawdown log-derivative signal without pump disturbance (A_1, A_2, A_3 and A_4), the derivative signal when pumping rate increases occur (B_1, B_2, B_3 and B_4) and the signal that is disturbed by a pump shut-down (C_1, C_2, C_3 and C_4). For both the change in pumping rate and the pump shut-down, similarly to the field observations in Fig. 2, the general trend of the derivative signal is rapidly recovered after the disturbance has stopped. In other words, the flow dimension value is temporarily disrupted by the pumping-rate disturbances but is not dependent on the pumping rate. Even when the test is altered during a short time period when a pumping rate change occurs, the general trend of the flow regime is not impacted. Furthermore, the step rate adjustments are generally observable during the test (induced peak noise) and have been considered in the interpretation of flow regimes.

As described by Eqs. (6) and (8), besides the hydraulic properties *K* and S_s of the aquifer and the extent of the flow zone *b*, the pumping rate *Q* is also a parameter that influences the derivative signal. We conducted several numerical tests to observe the impacts of the drift of the pumping rate on the flow dimension

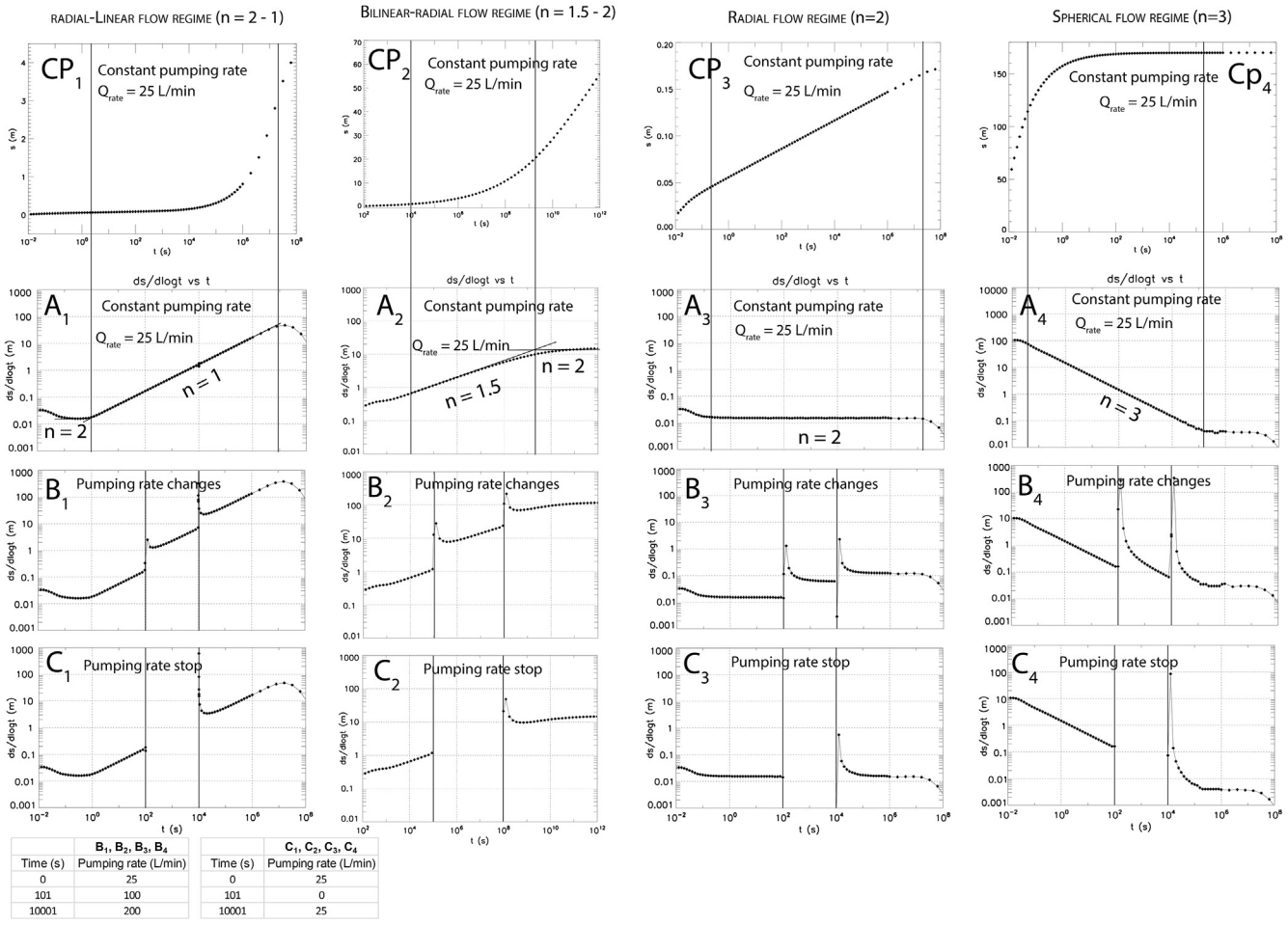

	B_1, B_2, B_3, B_4
Time (s)	Pumping rate (L/min)
0	25
101	100
10001	200

	C_1, C_2, C_3, C_4
Time (s)	Pumping rate (L/min)
0	25
101	0
10001	25

Fig. 3. Derivative signals of 4 conceptual models (one for each column) modeled numerically using HydroGeoSphere (Therrien et al., 2010). Respectively, the first, second, third and fourth column represent a radial-linear, bilinear-radial, radial and spherical-radial *n*-sequence. Respectively, the first, second, third and fourth line represent a semi-log plot of the *s* with a constant-rate pumping test (CP_i), the derivative signal with a constant-rate pumping test (A_i), the derivative signal with 3 increased adjustments of the pumping rate (B_i) and a derivative signal disrupted by a pump shut-down (C_i).

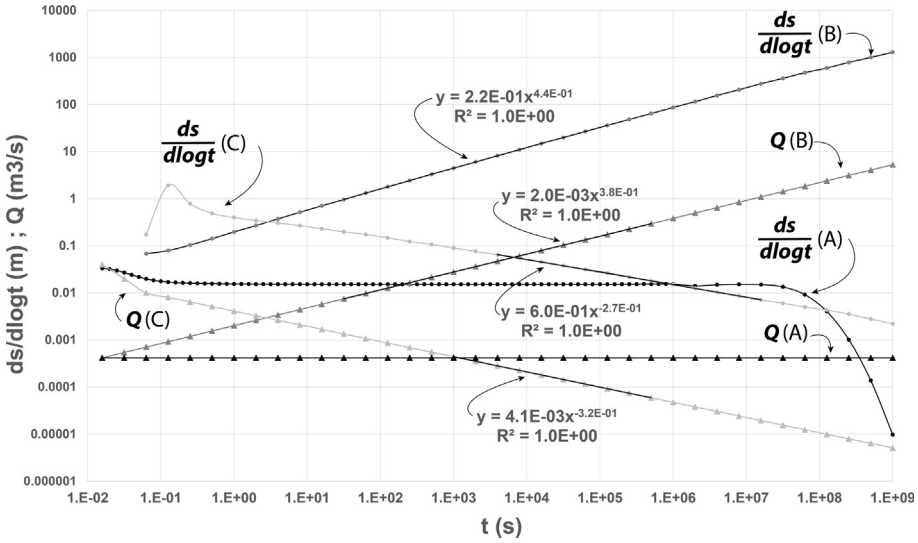

Fig. 4. A) 3 derivative signals associated with 3 different behaviors of the pumping rate of a same cylindrical-radial flow model modeled numerically using HydroGeoSphere (Therrien et al., 2010). The flow model is composed of an isotropic constant thickness aquifer bounded by constant head boundaries pumped by a vertical well located in the center. The solid lines with dots represent the drawdown log-derivative responses of the cylindrical-radial flow model induced by a particular pumping condition represented by dashed lines with triangles. *Q*(A) and *ds*/*dlogt*(A) are the curves of a constant rate pumping test and the associated derivative response, *Q*(B) and *ds*/*dlogt*(B) are the curves of an increasing power law pumping rate and the associated derivative response, and *Q*(C) and *ds*/*dlogt*(C) are the curves of a decreasing power law pumping rate and the associated derivative response.

value. Fig. 4-A shows numerical results of three situations of the drawdown log-derivative signatures of a cylindrical-radial flow model obtained in three different pumping rate conditions. In one case, the pumping rate is constant and in the two other cases we model a gradual drift of the pumping rate. In fact, the pump performance depends on the well head level. Fig. 4-A shows that the power law variation of the pumping rate influences the value of the flow dimension. The linear variation of the pumping rate induces an apparent flow dimension value which can be very different from the flow dimension of the equivalent constant-rate model. The slopes of the derivative signal and the pumping rate are practically identical (Fig. 4-A). According to the GRF model (Barker, 1988), the derivative signal is given by Eqs. (6) and (8). Because C is proportional to Q, when the pumping rate varies according to a power law (*i.e.*, $Q = Q_0.t^a$), Eq. (8) can be written as (Eq. (10)):

$$\frac{ds}{dlogt} = \frac{C'.v.t^v.Q_0.t^a}{2.3}. = \frac{C'.v.Q_0.t^{(v+a)}}{2.3} \tag{10}$$

With C′ written as (Eq. (11)):

$$C' = \frac{1}{4\pi^{1-v}Kb^{3-n}v}\left(\frac{4K}{S_s}\right)^v \tag{11}$$

With a the slope of the power law pumping rate drift $Q(t) = Q_0.t^a$. Thus, the slope p of the derivative response plot on a log-log graph is (Eq. (12)):

$$p = a + v = 1 + a - \frac{n}{2} \tag{12}$$

Consequently, the apparent flow dimension n_{app} induced by a power law pumping rate drift can be written as (Eq. (13)),

$$n_{app} = n - 2a \tag{13}$$

For instance, in Fig. 4-A, the slope of the increasing power law pumping rate a is equal to 0.38 and the related slope of the derivative signal is equal to 0.44, inducing an apparent flow dimension of $n_{app} = 1.12$ (calculated from Eq. (8)) instead of $n = 2$, which is the flow dimension of the constant-rate model. The apparent flow dimension calculated from Eq. (14) with the power exponent a of the variable flow rate is equal to $n_{app} = 1.24$. We observe a slight difference between the observed apparent flow dimension equal to 1.12 and the calculated apparent flow dimension equal to 1.24. These numerical tests are only a preliminary study which aims at issuing a warning to practitioners when interpreting the flow dimension, because pumping rate drifts can influence the flow dimension value. Obviously, further work is needed to suitably address the issue of pumping rate drift. In particular, other pumping rate drift behaviors should be analyzed. Unfortunately, the possible distortion of the flow dimension in the database due to pumping rate changes cannot be verified because pumping rate changes during the pumping test were not sufficiently monitored.

3.3. Geological contexts

A distribution of lithological types in each investigated area is provided in Table 1. 49 % of the database originates from pumping test data compiled by Rafini (2008) and 51 % from data collected within the framework of the PACES project (*Programme d'acquisition de connaissances sur les eaux souterraines*, a groundwater knowledge-acquisition program funded by the Ministry of Environment of Quebec and in part directed by the *Université du Québec à Chicoutimi*.

The Quebec bedrock is mainly composed of Precambrian crystalline rocks, essentially orthogneisses, paragneisses, granitic intrusions, anorthosite, and charnockites (Rondot, 1989). The crystalline rocks are disconformably overlaid by non-deformed sedimentary deposits composed, from depth to surface, of limestone to limy limestone, sandstone and shale (Lemieux et al., 2003). The limestones generally display a tabular lamination and may include clay interbeds. The carbonate rocks are today found only in the valleys or topographic depressions, where they have been protected from the intense erosion that occurred during the late Quaternary glaciation. The crystalline bedrock is interspersed by a complex fault system generated by various successive geological events dating from the Precambrian. Thick sand and gravel horizons overlaying the bedrock are found throughout the province of Quebec as the result of the late Quaternary glaciation. Various glacial and fluvio-glacial structures, such as tills, terminal and lateral moraines, eskers, kame, fluvio-glacial deltas, kettles, drumlins and floodplains compose the alluvial landscape of the region. The glacial retreat generated numerous eskers, particularly widespread in the Abitibi-Temiscamingue region (Quebec). These deposits, established by intra-glacial meltwater streams in ice tunnels, generally present a channelized structure and a stream-rate stratification (Levasseur, 1995). Marine transgression and regression events led to the deposition of fluvio-marine horizons that are represented by a confining clay layer above the fluvio-glacial sediments (Levasseur, 1995).

In northern Tunisia, pumping tests were performed exclusively in carbonate rock aquifers composed of limestones from the Eocene period. That region is characterised by thick stratified strata and finely laminated carbonate rocks (Rafini, 2004). The media is affected by faults formed during the Upper Jurassic and the Cretaceous and reactivated during the Pyrenean and Alpine compressions. The fractured media manifests a negligible karstification and a low matrix porosity.

The carbonate rocks studied in France are located in Alpine and Pyrenean forelands, composed of dolomite, limestone and marls. The crystalline media, located in the regions of Lozère and Loire (France), are characterised by a deeply weathered surficial horizon composed of granitic sand and clay-rich materials whose general hydrodynamic behavior have been explained in detail by Lachassagne (2008), Lachassagne et al. (2011) and Dewandel et al. (2011). Some wellbore loggings have reached a horizon composed of fissured rocks or compact rocks underlying the pumped granitic sand aquifer (BRGM database).

3.4. Comparison of hydraulic property values estimated from various models

In this section, the conventional Theis and Cooper-Jacob methods and a derivative analysis based on the cylindrical-radial flow regime are applied in various conceptual models. Some models display a long-term radial flow regime, whereas others show a sequence of radial and non-radial flow regimes. This analysis, composed of numerical and field data, aims at comparing the estimated hydraulic properties and to appreciate their degree of uncertainty when using the analytical models derived from the cylindrical-radial flow regime assumption.

Four conceptual models are modeled with a constant-rate pumping test. These conceptual models generate the following n-sequences: radial-linear, bilinear-radial, single-stage radial and spherical-radial flow regimes that are described in Section 2.2. The parameter estimation is performed using a manual type-curve matching: the Theis method (Theis, 1935), and two graphical analyses: the Cooper-Jacob semi-log method (Cooper and Jacob, 1946) and the radial derivative analysis. The Theis and the Cooper-Jacob solutions are described in Kruseman and Ridder (1994). The cylindrical-radial derivative analysis estimates the hydraulic conductivity for a cylindrical-radial flow regime using the following equation (Eq. (14) which is derived from Eq. (2)):

$$K = \frac{2.3Q}{m4\pi b} \quad (14)$$

with m [L] the Y-intercept of the radial flow dimension on a log-log plot of $ds/dlogt$ and b [L] the thickness of the cylindrical-radial cross-flow area. For each conceptual model, the log-log plot of the drawdown derivative signal is analyzed in order to identify the radial portion of the signal and to determine m.

The values of the hydraulic conductivity K are shown in Table 2. The grey lines in Table 2 represent the relative errors between the above K value and the modeled K value. The simplified diagrams of the Table 2 represent, from left to right, the semi-log plot of s *versus* t of the linear, the bilinear, the cylindrical-radial and the spherical flow dimension. When the conceptual model induces a single-stage cylindrical-radial flow regime, the three methods give a good approximation of K (the relative error ranges between 0 % and 6 %, Table 2). For the radial-linear, bilinear-radial and spherical-radial flow regimes, the type-curve matching and the graphical analysis of conventional methods are difficult to apply because the cylindrical-radial flow regime represents only a small portion of the entire signal.

The Cooper-Jacob plot of the linear flow (Fig. 3-CP_1) emphasizes two slopes. The first slope slightly underestimates K (−13 %), whereas the second slope strongly underestimates K (−99 %) or can be inadequately interpreted as a no-flow boundary. The derivative signal shows a short cylindrical-radial flow regime at early times before the long-term linear flow regime. This early times cylindrical-radial flow, reflecting the cylindrical diffusion of the cross-flow area before reaching the impermeable wall of the conduits, makes it possible to accurately estimate K with a relative error of −1 % (Table 2). Similarly, the semi-log plot of the spherical flow regime shows two slopes for the same flow regime. Both strongly underestimate K, probably because, in addition to not complying with the cylindrical-radial flow regime, the thickness that is investigated by the cross-flow area is different from the real thickness of the aquifer. The derivative signal (Fig. 3-A_4) shows a short radial flow regime at late times (unnoticeable in the semi-log plot of s). The radial flow regime, representing the reach of both the bottom and the top of the aquifer, makes it possible to estimate a good approximation of K with a relative error of 11 % (Table 2). Overestimating the hydraulic conductivity of the matrix K_m using the Theis and Cooper-Jacob models for the bilinear conceptual model is not surprising because these models assume a homogeneous aquifer and do not take into account the hydraulic conductivity of the fault K_f. The radial flow regime that is observed after the bilinear flow regime (Fig. 3-A_4) represents the "matrix-related radial flow regime" (Rafini and Larocque, 2012). This radial stage gives a good approximation of K_m using Eq. (14). The Cinco-Ley et al. (1978) solution developed for the vertical fault has the advantage of producing a value for K_f. To conclude, the K values estimated from the radial derivative analysis are close to the modeled K value. The relative errors are respectively 0 %, −1 %, 4 % and −25 % for the radial, radial-linear, the bilinear-radial and the spherical-radial conceptual models. The derivative signal has the advantage of clearly highlighting the radial flow regime by a flat horizontal slope of $ds/dlogt$.

We also analyzed two sets of field data (obtained from the Sainte-Anne and the Saint-Eustache wells) in order to compare the K values estimated from the four methods that were used in the previous section (Table 3). The wells are installed in fractured carbonate rocks. Field observations (such as packer tests) have highlighted the presence of conductive structures (Lemieux et al., 2006). The two derivative signatures (Fig. 5) show a multi-staged signal composed of the characteristic n-sequence 4-1.5-2, reflecting a non-connected vertical fault media (Rafini and Larocque, 2012). The K values estimated for the two pumping tests are close, regardless of the method used. This similarity in the results is probably related to the fact that the hydraulic conductivities of the matrix and of the fault are close to each other or the transmissivity of the fault is negligible compared to the transmissivity of the matrix.

Table 2
Hydraulic conductivity modeled and estimated from the Theis, Cooper-Jacob and radial derivative analysis for 4 conceptual models generating a radial-linear, a bilinear-radial, a radial and a spherical-radial flow regime. The grey lines represent the relative errors of the overlying K values. The derivative signals of the 4 conceptual models are shown in Fig. 3 (linear-A_1, bilinear-A_2 radial-A_3 and spherical-A_4). The simplified diagrams represent, from left to right, the semi-log plot of s vs t of the radial-linear, the bilinear-radial, the radial and the spherical-radial flow dimensions.

Flow regime		Radial-linear	Bilinear-radial	Radial	Spherical-radial
n-sequence		n = 2 - 1	n = 1.5 - 2	n = 2	n = 3 - 2
K (m/s) modeled		1.0E-05	-	1.0E-05	1.0E-05
K(matrix) (m/s) modeled for the bilinear-radial conceptual model (n = 1.5 - 2) *K(fault)_modeled = 1.0E-2 m/s ; bf = 2 m			1.0E-08		
K (m/s) estimated with the Theis method		1.9E-05	9.5E-08	9.5E-06	1.9E-08
		89%	***847%***	***-5%***	***-100%***
K (m/s) estimated with the Cooper-Jacob method	Semi-log plot of s vs t				
	First slope of s (p_1)	8.7E-06	7.4E-07	1.0E-05	4.4E-09
		-13%	***7267%***	***0%***	***-100%***
	Second slope of s (p_2)	9.3E-08	1.3E-08	-	1.1E-06
		-99%	***26%***	***-***	***-89%***
K (m/s) estimated with the radial derivative analysis	0 slope of $ds/dlogt$	9.9E-06	1.1E-08	1.0E-05	1.1E-05
		-1%	***12%***	***0%***	***11%***
K_matrix (m/s) estimated with the Cinco-Ley et al. (1978) solution for n = 2	0 slope of $ds/dlogt$	-	4.9E-09	-	-
		-	***-51%***	***-***	***-***
K_fault (m/s) estimated with the Cinco-Ley et al. (1978) solution for n = 1.5	0.25 slope of $ds/dlogt$ -> Kf	-	6.46E-06	-	-
		-	***-52%****	***-***	***-***

Table 3
Hydraulic conductivity values estimated from the Theis and Cooper-Jacob methods and the radial derivative analysis and for the *n*-sequence *n* = 1.5–2.

		Saint-Anne	Saint-Eustache
n-sequence		*n* = 4–1.5–2	*n* = 4–1.5–2
K (m/s) estimated with the Theis method	First fit	5.3E−04	5.2E−05
K (m/s) estimated with the Cooper-Jacob method	First slope of s	4.1E−04	4.2E−05
	Second slope of s	5.4E−04	3.5E−05
K (m/s) estimated with the radial derivative analysis	0 slope of *ds*/*dlogt*	4.8E−04	3.6E−05
*K*_matrix (m/s) estimated with the Cinco-Ley et al. (1978) solution for *n* = 2	0 slope of *ds*/*dlogt*	2.1E−04	1.6E−05
*T*_fault (m2/s) estimated with the Cinco-Ley et al. (1978) solution for *n* = 1.5	0.25 slope of *ds*/*dlogt* -> *Tf*	8.4E−03	3.4E−03

4. Results and discussion

4.1. Flow dimension versus Theis analysis: case studies

This section describes two different situations that illustrate the benefits of using flow dimension analysis in addition to drawdown-only conventional interpretations to better characterize the flow regimes induced by a pumping test.

4.1.1. Case study 1

Fig. 6 represents the semi-log plot of the drawdown signal (upper plots) and the bi-logarithmic plot of the drawdown log-derivative signal (lower plots) of a 3-day constant-rate pumping test conducted in the glacio-fluvial deposits of the Senneterre esker (Mirabel, Quebec, Canada). Despite the noise of the drawdown log-derivative signal between 100 min and 4230 min, the SIREN code makes it possible to assuredly fit a sub-radial ($1 < n < 2$) flow dimension by fitting at the same time both the semi-log plot of the drawdown (which is much less noisy) and the lower plot of the drawdown log-derivative signal. Using the traditional Cooper and Jacob method, the drawdown signal is interpreted by drawing two straight lines (Fig. 6-A): a first line from 0.3 to 230 min and the second line from 230 to 4320 min. The second straight line, whose slope is roughly double that of the first line, might be interpreted as a second media with a lesser transmissivity or as the attainment of impermeable boundary conditions. In a first approximation, these two successive straight lines appear as an acceptable linear regression. But when visualizing the effect of the fit of these two supposed radial flow regimes (upper plot of Fig. 6-A) on a log-log plot of *ds*/*dlogt* (lower plot of Fig. 6-A), we see two distinct horizontal straight lines which are obviously an inappropriate representation of the existing data points.

As shown in Fig. 6b, fitting a 0.35 straight line slope (*n* = 1.3, Eq. (4)) onto the *ds*/*dlogt* signal, resulting in a convex curve on the semi-log plot of *s*, represents the real data much more accurately.

The pumping test is performed in an esker, a fluvio-glacial sedimentary feature that typically contains channels (Escobar et al., 2004a; Corbett et al., 2012). Such channels impede the cross-flow area to laterally expand during drawdown diffusion. Remaining constant in these alluvial conduits, the flow dimension of eskers is expected to be linear. However, each of the seven derivative signals of eskers that have been analyzed in this database showed a sub-radial flow dimension (*n* = 1.3). We interpret this sub-radial flow dimension to be related to leakage coming from the surrounding deposits and that supplies the highly transmissive esker conduit. This assumption is further explained in the general discussion section.

Using the Cooper and Jacob model in this case would lead the practitioner to interpret the data as representing a Theis aquifer bounded by an impermeable boundary (Ferris, 1949). But Cooper-Jacob is not a valid model to interpret this pumping test. Rather, the flow dimension analysis, which fits the data and the conceptual model much more closely, is able to detect the presence of a sub-radial flow regime.

This case study illustrates how the identification of flow regime sequences rather than the trivial postulate of a radial flow regime may substantially improve the diagnosis of the aquifer's hydraulic properties, a diagnosis which exerts numerous practical implications on resource management (*e.g.*, a wellhead protection area (WHPA) delineation).

4.1.2. Case study 2

Fig. 7 represents 3 different examples of pumping test interpretations of a 6.5 day constant-rate pumping test performed in a carbonate rock aquifer in the Sainte-Anne-des-Plaines site (Mirabel, Quebec, Canada). The same methodology as the one that is used in case study 1 is adopted. The reliability of the fitting of the *s* data (upper plots of Fig. 7-A-B-C) is checked by analysing the match with the *ds*/*dlogt* signal (lower plots of Fig. 7-A-B-C). As shown in Fig. 7-A and B, neither a long radial flow regime

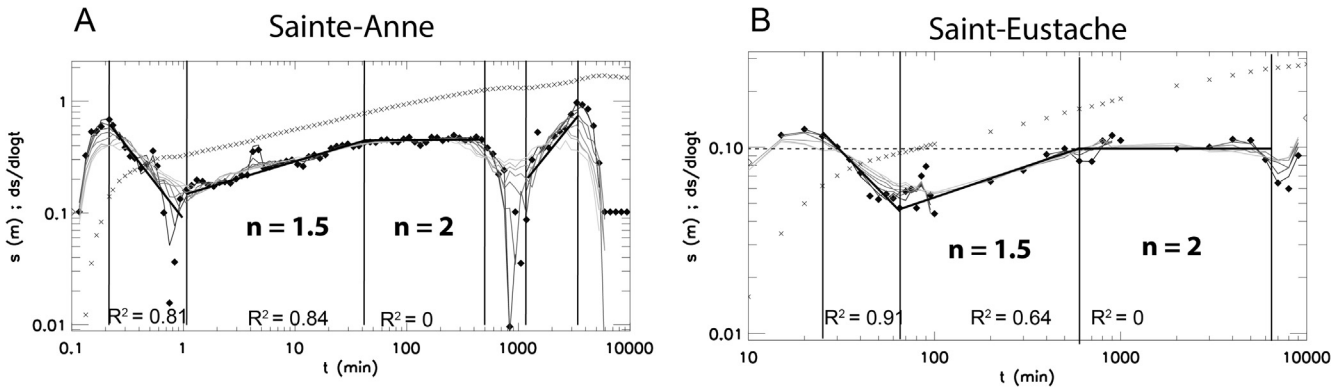

Fig. 5. Diagnostic plots and flow regime interpretations in fractured rock aquifers. A: constant-rate pumping test (6.5 days) conducted in the P-8 well located in a Chasy carbonate rock aquifer of Sainte-Anne-des-Plaines (Charlevoix, Quebec, Canada). B: constant-rate pumping test (6.5 days) conducted in the SE6 well located in the aquifer of Saint-Eustache composed of the Beauharnois rock unit (Mirabel, Quebec, Canada). The diamond shapes represent the drawdown log-derivative signal and the "x" shapes represent the drawdown signal. The R^2 value represents the coefficient of determination between the derivative data and the regression line.

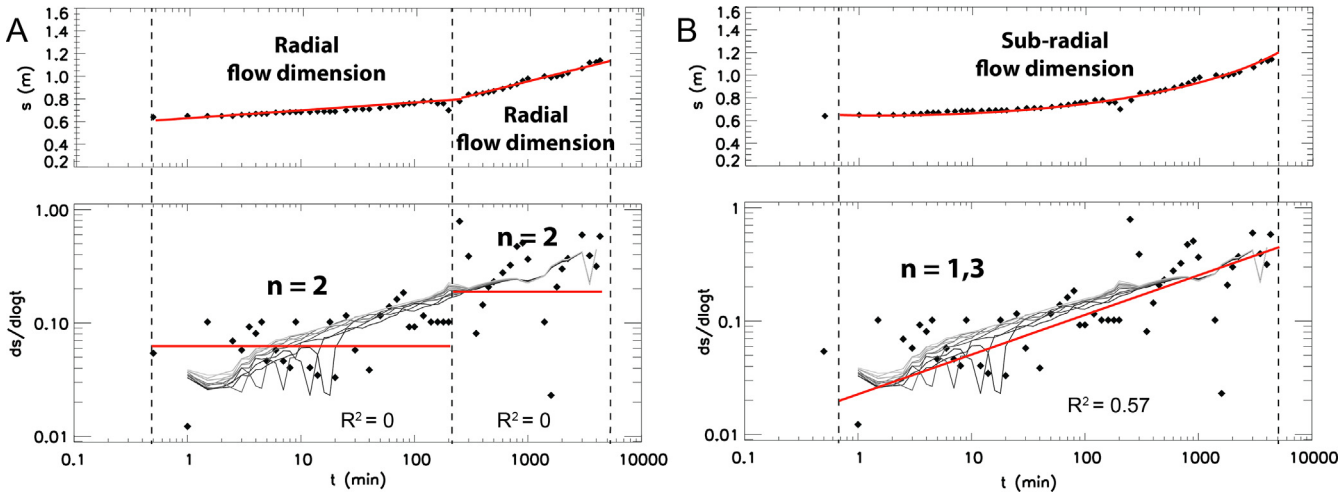

Fig. 6. Diagnostic plots and interpretations of a constant-rate pumping test conducted in the PP-1 well located in the fluvio-glacial deposits of the Senneterre esker (Mirabel, Quebec, Canada). In the upper part of figures a) and b): Semi-log plot of the drawdown *s*; in the lower part: log-log plot of the drawdown-log derivative *ds*/*dlogt*. A) Example of a conventional interpretation assuming radial flow regimes, B) Demonstration of a more accurate interpretation of the pumping test using a *ds*/*dlogt* log-log plot. The grey lines, derived from the algorithm of Bourdet et al. (1989), represent seven data smoothings for *L* ranging between 0.2 and 0.8. The R^2 value represents the coefficient of determination between the derivative data and the regression line.

(from 1,8 to 400 min, Fig. 7-A), neither two successive radial flow regimes (one from 1,5 to 30 min and another from 30 to 400 min, Fig. 7-B) can adequately reproduce the trend of both the *s* and *ds*/*dlogt* signatures. Even if the match of 1 or 2 radial flow regimes seems to be a rather good approximation on the semi-log plot of *s*, the linear regression is visibly inconsistent on a *ds*/*dlogt* log-log plot.

A much more suitable fit of *s* and *ds*/*dlogt* is presented in Fig. 7-C where the signal is divided in a sequence of flow regimes with various *n* values. On a semi-log plot of *s*, values of $n < 2$, $n > 2$, and $n = 2$ show respectively a convex, a concave and a straight curve reflecting a rising, a declining or a static drawdown rate. Conceptually, these flow regimes can be related to transmissivity patterns. Bowman et al. (2012) showed numerically that $n < 2$ and $n > 2$ may be generated by conduit geometry in which the cross-sectional area respectively decreases and increases as a power function of distance. Finally, for $n = 2$, the derivative horizontally straightens and the drawdown signal displays a straight line, indicating no change in the drawdown rate, which agrees with the Cooper-Jacob model.

The *ds*/*dlogt* signal displays a sequence of integer and non-integer flow regimes (Fig. 7-C): a fractional flow regime ($n = 1.5$ from 1.8 to 40 min), followed by a radial flow regime ($n = 2$ from 40 to 500 min). This *n* sequence composed of $n = 1.5$ and $n = 2$ has been numerically shown by Rafini and Larocque (2012) to be generated by the presence of a vertical finite-conductivity fault embedded into an aquifer, and not directly connected to the pumping well. The $n = 1.5$ segment represents a bilinear flow regime indicating that the pressure front pulse expands through a media composed by a finite-conductive fault and the fractured rock continuous-like matrix (Abbaszadeh and Cinco-Ley, 1995; Rafini and Larocque, 2009). In other words, during the constant-rate pumping test, the fault that is supplying the well is at the same time supplied by the matrix, inducing a diffusion deceleration that is responsible for the fractional flow regime occurrence (Rafini and Larocque, 2009). The radial flow is observed following the bilinear flow regime and indicates that the pressure front pulse diffusion through the matrix is dominant over the pressure front pulse diffusion through the fault. The influence of the fault is thus totally masked by the matrix's hydraulic response, which predominates over the aquifer's response So far, the leaky vertical fault is the only flow model that has been documented to interpret $n = 1.5$. If the area of the cross flow undergoes a change which is proportional to $r^{0.5}$, this will produce a value of *n* equal to 1.5.

This case study provides another example showing that interpreting pumping test data using the traditional drawdown analysis on semi-log plots leads the practitioner to miss most of the information and to perform an invalid or low-quality hydrodynamic diagnosis. Such inappropriate interpretation of flow will induce inaccuracies in the estimation of the aquifer's hydraulic properties. For instance, assuming a radial flow ($n = 2$) in a homogeneous media while the aquifer is, in fact, composed of a vertical fault that generates a bilinear flow ($n = 1.5$), would lead the practitioner to overestimate the matrix's transmissivity, to ignore the presence of a water-bearing fault or to underestimate the fault's transmissivity.

4.2. The occurrences of flow dimension in natural aquifers

The scope of this section is to provide an overview of the occurrence of flow dimension in nature and to compare the values of *n* against their geological settings in order to obtain insights into the physical meaning of flow dimension in terms of what it can tell us about the hydrogeological settings and features. Note that only derivative slopes which rigorously correspond to a flow dimension are retained. Slopes more likely relating to transitions and boundary effects (no-flow or constant head) were not included in the database. In fact, as defined by Barker (1988), the flow dimension must reflect the properties of a volume of aquifer investigated by the cross-flow area. This definition of the flow dimension will be covered in the discussion section.

4.2.1. Analysis of the entire database

4.2.1.1. Flow dimension values. The database contains data from 69 well tests conducted in three different geological environments, in roughly the same proportions: crystalline rocks (19 pumping tests), carbonate rocks (28 pumping tests) and alluvial deposits (22 pumping tests). The pumping tests were performed on average during 2.5 days (63 % of the tests ranged from 2 to 4 days). The four shortest well tests lasted 4 h, 5.5 h, 12 h and 15 h, whereas the four longest well tests lasted 7.1 days, 8 days, 9.1 days and 14.7 days.

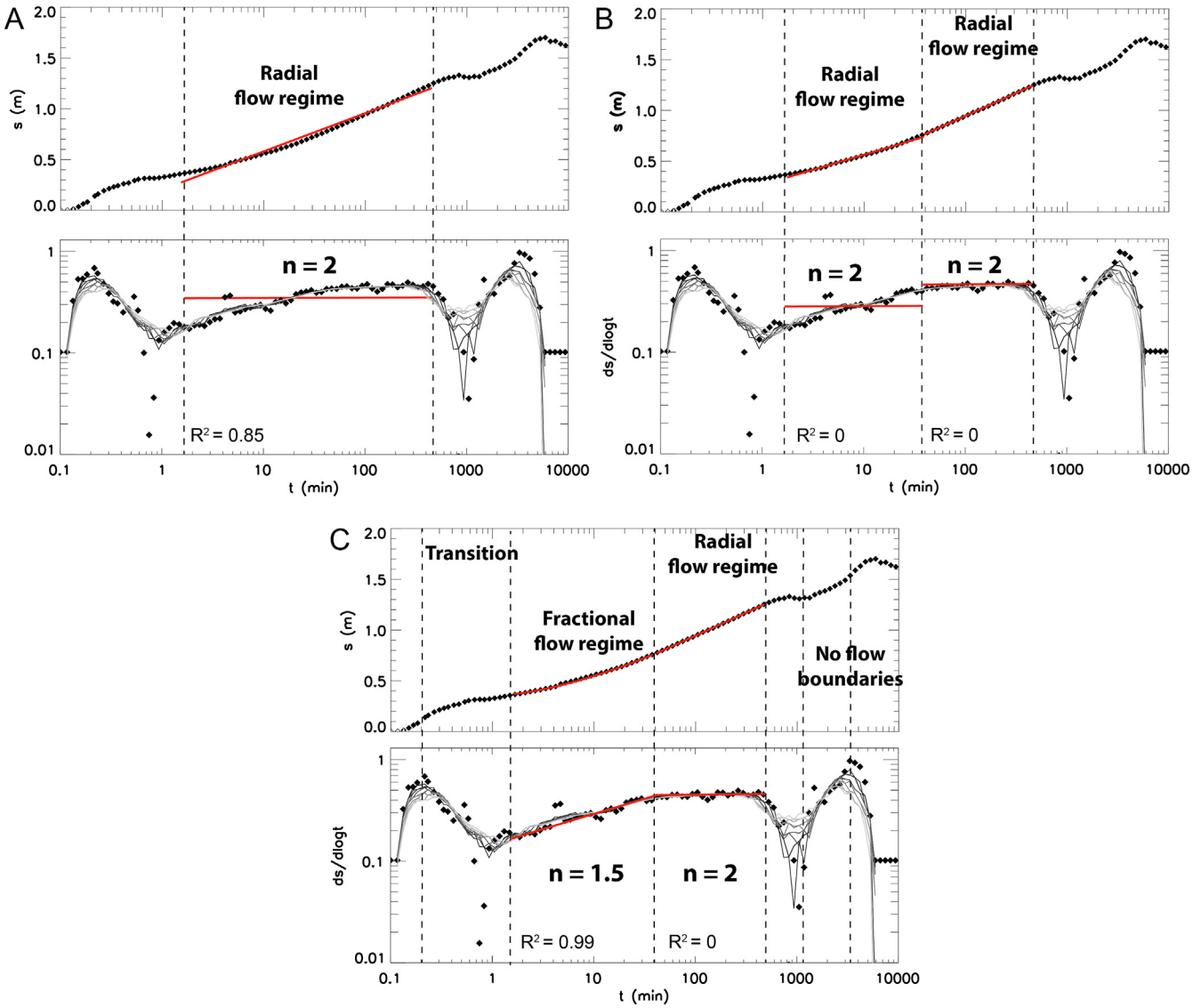

Fig. 7. Diagnostic plots and interpretations of a constant-rate pumping test (6.5 days) conducted in the P-8 well located in a Chasy carbonate rock aquifer of Sainte-Anne-des-Plaines (Charlevoix, Quebec, Canada). In the upper part of Figures A), B) and C): Semi-log plot of the drawdown *s*; in the lower part of the same figures: log-log plot of the drawdown-log derivative *ds*/*dlogt*. a) Hydrodynamic analysis assuming one radial flow regime, b) Hydrodynamic analysis assuming a sequence of two radial flow regimes, c) Hydrodynamic analysis assuming a sequence of a fractional and a radial flow regime. The grey lines, derived from the algorithm of Bourdet et al. (1989), represent seven data smoothings for *L* ranging between 0.2 and 0.8. The R^2 value represents the coefficient of determination between the derivative data and the regression line.

Analysis of the data from these 69 pumping tests provided flow dimension distribution values ranging between 0.2 and 3.5, with a mean value of 1.7 and a standard deviation of 0.4. Other studies have also analyzed the frequency of occurrence of the flow dimension from field data (Table 4). The frequencies of occurrence of *n* posited by the studies of Bangoy et al. (1992), Kuusela-Lahtinen et al. (2003), Audouin and Bodin (2008) and Verbovšek (2009, 2011) bring valuable insight as to how *n* occurs in fractured rock aquifers. Each of these 4 studies, however, is restricted to only one or two fractured rock settings and used *n* as a tool for refining the characterization of fractured media or to help in selecting the analytical model. Only one (Verbovšek, 2009, 2011) presented a statistical study aiming to analyse the influence of several parameters on *n*, such as the lithological properties of dolomites, their age, the topographical settings, the degree of penetration of the wells, *etc*. His study analyzes the statistical occurrence of *n* in a single geological setting, the dolomites. Our study compared *n* to various environments such as crystalline and carbonate fractured rocks, weathered crystalline rocks and fluvio-glacial deposits in order to better understand the relationship between *n* and the local geological features. Because statistical studies examine and manipulate direct field information, they contribute information in parallel to numerical studies and make it possible to enrich our physical interpretation of *n*.

Because the data used for the studies of Table 4 were obtained by means of various different methodologies to conduct pumping tests (packer test, slug test, pumping test) and a wide diversity of procedures to determine flow dimensions (manual and automated type-curve matching of *s* or *ds*/*dlogt*, sequential analysis of *ds*/*dlogt*), the studies should be compared with caution. Indeed, the pumping test duration scale is different for all studies, implying that the portion of each aquifer investigated by the pressure front pulse is no doubt variable. We should remember that short-term pumping test studies are only capable of expressing wellbore effects and the behavior of the aquifer in the area closest to the well.

Table 4
Summary of studies analysing the frequency of occurrence of the flow dimension n.

Type of test	Range of n	Geological setting	Nb of pumping wells	Duration of the pumping test	Location of pumping tests	Methodology	Reference
Pumping test	$0,2 < n < 1,34$	Granitic rock and carbonate rock aquifers	2 pumping wells, 12 observation piezometers	25 h (granitic rock aquifer), <10 h (carbonate rock aquifer)	Pyrenee (southern France), Terrieu (France)	Type-curve fitting of s	Bangoy et al. (1992)
Hydraulic tests	76 % of the data showed fractal n, with $1 < n < 2$	54 fractured aquifers	126 well tests		Korean		Hamm (1995)
Three multiple constant rate pumping tests	$1,6 < n < 2$ for the pumped fracture zone and $n = 1,45–1,5$ in the neighboring one	Poorly weathered crystalline rocks. No flow in the crystalline matrix. Intense fracturing along subvertical Precambrian shear zones	3 pumping wells, 4 observation piezometers	6 h of pumping	Leppavirta (south–central Finland)	Best-fitting curve based on an analytical model with fractional flow dimensions	Leveinen (2000)
Pressure-pulse, constant-pressure flow, pressure-recovery tests	$1 < n < 3$	Evaporite deposits	16 hydraulic tests	not determined	Waste Isolation Pilot Plant of the Delaware Bassin (New Mexico)	Type-curve fitting	Beauheim et Roberts (2002)
2 m and 10 m constant pressure injection test	$1,6 < n < 2,5$	Low conductivity crystalline rock aquifer	5 pumping wells, 175 constant-pressure injection tests	around 1 h or less	Romuvaara (Suede)	Type-curve fitting of ds/dlogt (FRACDIMQ algorithm, Doe et Geier 1990)	Kuusela-Lahtinen et al. (2003a)
Constant-rate pumping tests	$n = 1,6$	Crystalline aquifer (preferential weathering of a subvertical fractured zone)	106 m3 per year since 1991 as the main water supply for a town of 20,000 inhabitants	3 pumping tests, whose duration was 5, 13 and 88 days, with sampling rates as short as 1 min, giving a scale range of 4–5 orders of magnitude in time	Plœmeur	Best-fitting of both s and ds/dlogt	le Borgne et al. (2004)
Step drawdown test	2,25	Fractured limestones	1 pumping well	approximately 150 min	Montpellier University yard (France)	Type-curve fitting of the semi-logarithmic plot of the drawdown data (with a leakage model)	Lods and Gouze (2004)
Pumping tests	0,7	Fractured rock (harzburgite massif)	1 pumping well	approximately 80 h	Ophiolitic complex of Oman	Type-curve fitting of the semi-logarithmic plot of the drawdown data (with a double porosity model)	Lods and Gouze (2004)
Pumping tests	1,7	Fractured rock (gabbros)	1 pumping well, 3 observation piezometers	around than 80 h	Ophiolitic complex of Oman	Type-curve fitting of the semi-logarithmic plot of the drawdown data	Lods and Gouze (2004)
Pumping tests	1,8	Fractured granites	1 pumping well, 3 observation piezometers	around 16 h	South Centre of India	Type-curve fitting of the semi-logarithmic plot of the drawdown data (with a model composed of a fracture and a matrix)	Lods and Gouze (2004)
Pumping tests	1,45	Fractured granites	1 pumping well, 1 observation piezometer	less than 20 h of pumping	South Korea	Type-curve fitting of the semi-logarithmic plot of the drawdown data (with a leakage model)	Lods and Gouze (2004)
Pumping tests	$1,2 < n < 2$	Weathered crystalline rock aquifer (3 m of underlying horizontally fractured-weathered layer)	34 pumping wells/ observation wells	around 1 day	Maheshwaram watershed (India)	Type-curve fitting of the semi-logarithmic plot of the drawdown data	Maréchal et al. (2004)

(*continued on next page*)

Table 4 (*continued*)

Type of test	Range of n	Geological setting	Nb of pumping wells	Duration of the pumping test	Location of pumping tests	Methodology	Reference
Slug test	1,6 < n < 2,5	Fractured and karstic limestone aquifers	13 pumping wells	around 100 s	Hydrogeological Experiment Site; Poitier (France)	Automatic inversion algorithm	Audouin and Bodin (2008)
Pumping tests	1 < n < 3	Dolomite aquifers	72 pumping wells	around 50 h	Slovenia	Automatic best-fitting of both s and ds/dlogt	Verbovšek (2009, 2011)
Interference tests	1,25 < n < 2	Fractured aquifer with thrust faults	1 pumping well, 4 observation piezometers	several tests from 18,5 to 258,5 h	Chinghsui geothermal reservoir (Northeast of Taiwan)	Best fitting of the σ function	Liang et al. (2012)
Constant-rate pumping tests	2,21 < n < 2,38	Chalk aquifer	4 pumping well	47 h	Wilfholme landing on the Holderness plain of east Yorkshire (NE England)	Best-fitting of both the drawdown data	Odling et al. (2013)
Constant-rate pumping tests	0 < n < 3,4	Fractured crystalline and carbonate rock aquifers, weathered crystalline rock aquifers, fluvio -glacial deposit aquifers	70 pumping wells	around 72 h	Quebec, France, Tunisia	Manual fitting of both s and ds/dlogt	This study

Fig. 8 shows the occurrence of frequency of n in the entire database (not considering the duration of observation of n). The figure shows that there is a wide diversity of n values. In particular, the large clear bars of Fig. 8 show that the linear, radial and spherical dimensions represent, respectively, 20 %, 31 % and 8 % of the 121 flow dimensions analyzed. Non-integer n values are also significantly represented. The fractional n values in ranges 0–1, 1–2, 2–3 and >3 represent, respectively, 3 %, 24 %, 11 %, and 1 % of all n values, which together amount to a total of 38 % of fractional flow dimension values.

Radial flow regimes are observed in 55 % of the 69 pumping tests and represent 31 % of the 121 flow regimes that were interpreted overall (large bars in Fig. 8). These radial flow regime occurrences are observed systematically in a sequence of several flow regimes with non-radial flow dimensions. As a result: i) the unique radial flow conditions as stipulated by Theis are rarely observed in this database; ii) radial flow is observed only 31 % of the overall reported flow regimes, while it is assumed in an overwhelming majority of existing interpretative models. In fact, most analytical models published in the petroleum literature since the 80's are variations on the radial theme. The fact that we are now able to observe predominantly non-radial flow dimensions emphasizes the need to develop interpretative models that represent the real dimension of flow more accurately than Theis and Theis-derived models, which remain commonly used.

It is interesting to note that the n values smaller than 2, equal to 2 and greater than 2 are associated with different flow behaviors: $0 < n \leq 2$ is related to an increase of the drawdown rate (thus, the head decline accelerates), while $n > 2$ expresses a decline of the drawdown rate (thus, the head decline decelerates). A summary of the hydrodynamics of each class is given in Table 5. Based on the Barker relation (Eq. (1)), the n values ranging between 0 and 1 are interpreted as a decrease of the cross-flow area as it expands radially. This can suggest a reduction of the transmissivity as the pressure-front pulse expands or, for $n = 0$, a depletion of the aquifer. The n values equal to 1 are associated with a cross-flow area that is constant (Eq. (1)), suggesting that the pressure wave is diffusing through a channelized environment, as explained above. All the values of $n > 1$ express an increase of $A(r)$ (Table 3) that is induced by various geometries of boundaries, transmissivity configurations, fault-matrix relations, *etc.* (cf. Section 2.2.2).

4.2.1.2. Flow regime duration. The duration of flow regimes is a critical point of the flow dimension analysis. This issue was addressed by computing the "mean of the logarithmic duration of n", calculated as follows: (the number of observation of n of a pumping test) * ($\sum$ of the logarithmic duration of n of a pumping test)/($\sum$ of the logarithmic durations of n of the entire database).

The thin dark bars of Fig. 8 represent the mean of the logarithmic duration of n (right axis) and the large bars of Fig. 8 show the frequency of occurrence of n (left axis). Presenting these two types of information in combination shows that the most frequently observed flow dimensions are not necessarily the longer-lasting ones. In fact, the thin dark bars show that the most stable long-term flow dimensions are $n = 2.4$, $n = 1.3$ and $n = 1.6$, which are observed during respective averages of 2.36, 2.28 and 2.17 log-cycles. The sub-radial flow dimension ($n = 1.3$), which is almost exclusively observed in alluvial deposits, is observed during a long-lasting duration (2.3 log-cycles in average). The bilinear flow dimension ($n = 1.5$), mostly observed in fractured rocks, is observed during 1.9 log-cycle on average. On the contrary, the radial flow dimension $n = 2$ is one of the most frequent flow dimensions of the database (31 % of the 121 flow dimensions) but it is also one of the shortest-lasting flow dimensions. On average, $n = 2$ is observed during less than one log-cycle (0.97 log-cycle in average). In fact, in all the various geological settings, $n = 2$ has gener-

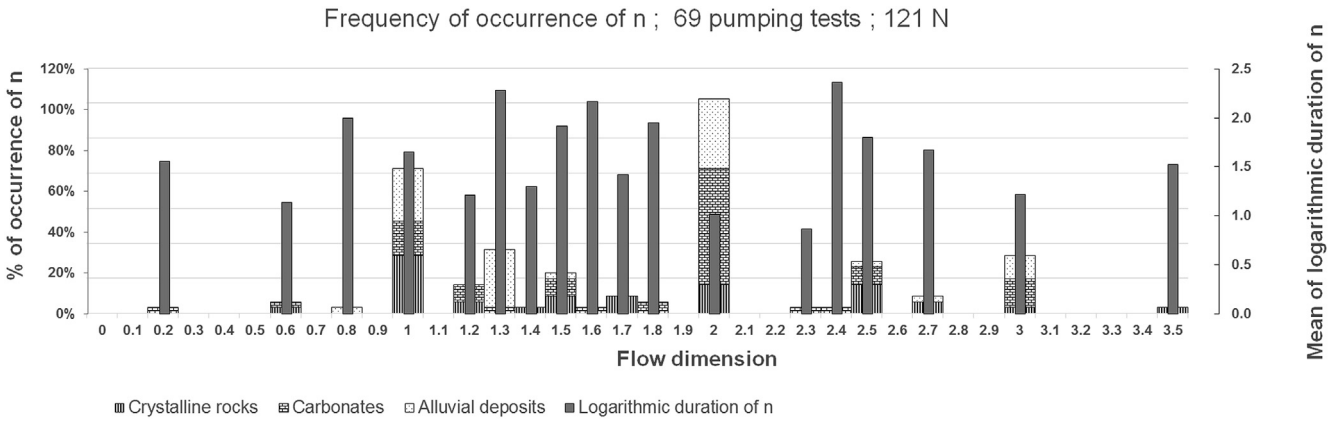

Fig. 8. Statistical analysis of the flow dimension occurrence during 69 constant-rate pumping tests (including respectively 19, 22 and 28 pumping tests in fractured rocks, deposits and carbonate rocks), located in Canada, France and Tunisia. The database contains 121 distinct flow dimension values. The "N" in the graph titles represents the number of observed flow dimensions. The flow dimension is manually estimated from a sequential analysis. The large bars are read on the left y-axis, the thin-dark bars are read on the right y-axis.

Table 5
Summary of hydrodynamic interpretations of n and their graphical representations.

Flow dimension n	$n < 1$	$n = 1$	$1 < n < 2$	$n = 2$	$n > 2$
Cross-flow area $A(r)$	↘	→	↗	↗	↗
Log-rate of drawdown s	↗	↗	↗	→	↘
Shape of s on a semi-log plot	convex curve	convex curve	convex curve	straight line	concave curve
Shape of $ds/dlogt$ on a log-log plot	rising slope	rising slope	rising slope	horizontal slope	declining slope

↗: increases when r ↗.
↘: decreases when r ↗.
→: is constant when r ↗.

ally been observed at the beginning of the pumping tests and during a short time period. The linear flow dimension ($n = 1$) is also related to a long-lasting signal (1.7 log-cycles in average) and is observed in equal proportions between the alluvial deposits (7 %), the carbonates (8 %) and the crystalline rocks (5 %). Insights on the conceptual interpretation of the observed flow dimensions are given in the following section by combining the values and the duration of n and the geological settings.

This figure also shows some relationships between the n values and the geological environments. For instance, $n = 1.3$ is exclusively observed in alluvial deposits, while $n = 1.5$ and $n = 2.5$ are almost exclusively observed in fractured rocks. The affinity of n to certain environments suggests that the geological facies influences the geometry of the pressure wave, and so the flow dimension. It may be thus a valuable tool to explore the properties of the aquifer that control the flow regimes.

4.2.1.3. Flow dimension sequences. The flow dimension values included the database are only those that are assumed to be representative of the properties of a volume of aquifer. However, the flow dimension sequence takes into account every slope of a signal. Thus, for certain signals, the wellbore effects, transitions and/or hydraulic boundaries are considered into the sequence.

Most signals exhibit several successive flow regimes marked by different n values: 88 % of the pumping tests analyzed for this study were multi-stage, with 38 %, 44 % and 6 %, presenting, respectively, 2, 3 and 4 sequences of flow dimensions (Fig. 9). The n sequences express various geological facies that control the pressure wave and which are successively reached by this pressure wave.

Fractured media produce a major proportion of n-sequential signals: they represent, respectively, 85 %, 100 % and 96 % of the pumping tests performed in faulted crystalline rocks, altered crystalline rocks and carbonate rocks. This suggests that fractured media are complex heterogeneous systems involving various flow regimes (Fig. 9).

At early times, a change of derivative slope may signal the evolution from wellbore and skin effects to the aquifer response. At middle times and late times, as the pressure front pulse expands through the aquifer, variable slope sequences of $ds/dlogt$ can express changes in the hydraulic and/or geometrical conditions of the aquifer, transitions and/or eventually the attainment of hydraulic boundaries. Note that the derivative signatures that are related to skin effects, wellbore storage effects or hydraulic boundaries have not been included in the flow dimension database.

Sequences of flow regimes have often been reported in various field and numerical studies conducted in fractured rock aquifers (Ehlig-Economides, 1988; Mattar 1997; Escobar et al., 2005; Renard et al., 2009; Rafini and Larocque, 2012). This study, based on an n-sequential analysis, further shows that, contrary to current opinion, alluvial deposits can also exhibit complex flow behaviors with discontinuous flow regimes and fractional n values (primarily ranging from 1 to 2).

A wide array of n values was observed in the database, in different sequences, of various durations and with varying frequencies of occurrence. The following section describes the results obtained when comparing the flow regimes to the geological environments of wells in order to obtain insights on the physical interpretation of n.

4.2.2. Analysis of the distribution of n in different geological environments

4.2.2.1. Crystalline rock aquifers. Based on 19 pumping tests, the frequency histogram of n in crystalline rock aquifers displays scattered and highly variable values. The faulted crystalline rocks (FCR) studied are located in Canada while the altered crystalline rocks (ACR) studied are located in France. Because the sequences

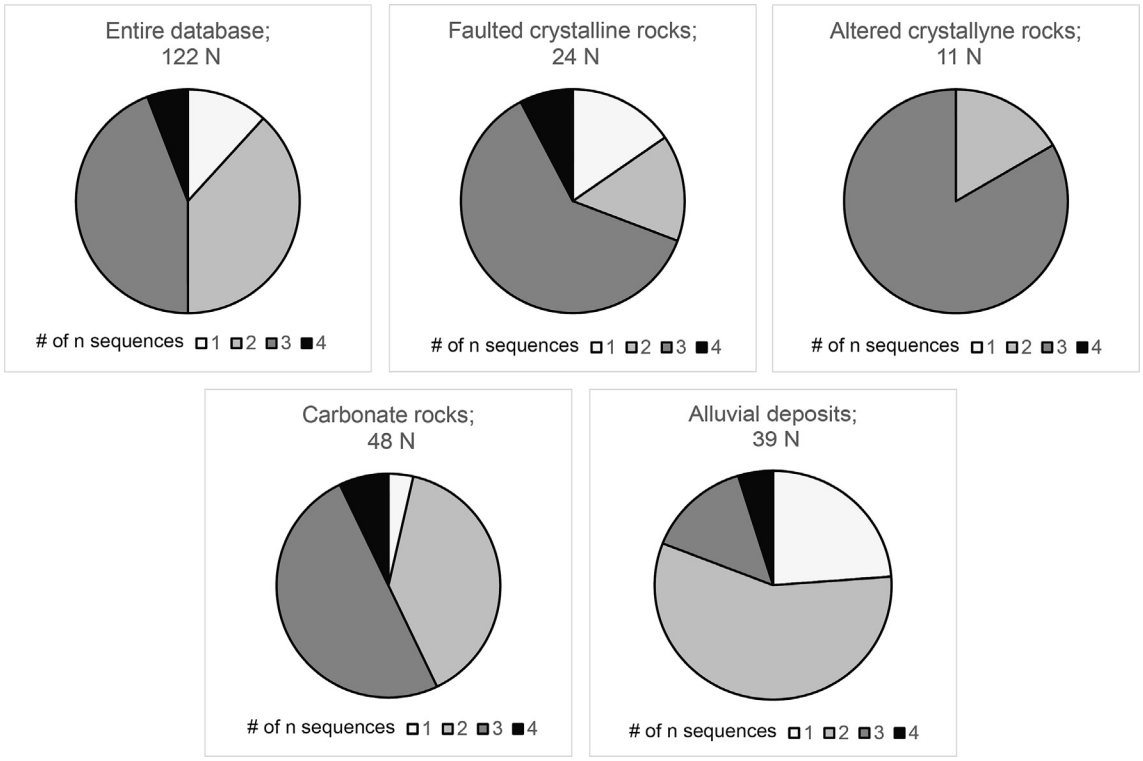

Fig. 9. Proportional distribution of the 1, 2, 3 and 4 *n* sequences in the 69 pumping tests conducted for this study.

and values of *n* are different between the 2 groups, they were analyzed separately.

The FCR group of pumping tests, which produced 24 distinct flow regimes with 13 pumping tests, showed various *n* values characteristic of long-lasting flow regimes. The most significant *n* values are 1 – 2.5 – 2 – 1.5, representing, respectively, 38 %, 21 %, 17 % and 8 % of the FCR *n*, and lasting, respectively, 1.6, 1.5, 0.9 and 2.7 log-cycles (Fig. 10-A).

The occurrence of linear ($n = 1$) and bilinear flow regimes ($n = 1.5$) in these environments corroborate their common conceptual interpretation as expressing the presence of conductive fractures: $n = 1$ has been attributed by Gringarten et al. (1974, 1975) to an infinite-conductivity fracture and by Cinco-Ley et al. (1978) and Cinco-Ley and Samaniego (1981) to a finite-conductive fracture (early pumping time). The first conceptual model assumes a matrix linear flow originating from the uniformly depressurized fault, which consequently acts as a planar source, while the second model stipulates a linear flow occurring into the fault before the embedding matrix is depressurized. The embedding environment is assumed to behave like a continuous porous media, which means that the fracture network is dense with a sufficiently high degree of connectivity. Obviously, any flow model that produces a diffusion of the cross-flow area that does not change with distance will produce a linear flow regime. Linear flow regimes may also be produced in hard rock aquifers from one-dimensional flow conduits formed at the intersection of two fractures or faults (Eq. (1)), in channels along the fault plane (Figueiredo et al., 2016) or when a fracture set controls the flow in one direction.

The value $n = 1.5$ has been associated with an aquifer composed of a vertical finite-conductive fault supplied by a continuous Theissian matrix with a hydraulic conductivity lower than the fault (Cinco-Ley et al., 1978; Cinco-Ley and Samaniego-V., 1981; Rafini and Larocque, 2012).

The fractional values of *n* which range between 1 and 2 (*e.g.*, $n = 1.2$ or $n = 1.7$) have not to this date been assigned a conceptual description (with the exception of $n = 1.5$). Some assumptions on the physical interpretation of sub-radial flow dimensions can however be made regarding the properties of faulted/fractured networks, the distribution of transmissivity around the well and the geometry of faults or boundaries. The only limitation is that the diffusion of the pressure disturbance must satisfy Eq. (1). For instance, as stated by Bowman et al. (2012), *n* is influenced either by the geometry of flow conduits or by leakage effects into the conduits. According to Raghavan (2004), a decreasing permeability with distance from the wellbore leads to an increase of the $ds/dlogt$ signal ($0 < n < 2$). Several authors have associated fractional flow dimensions to the scale-invariant properties of fracture networks (Chang and Yortsos, 1990; Bangoy et al., 1992; Acuna and Yortsos, 1995; de Dreuzy et al., 2000; Doughty and Karasaki, 2002; Walker et al., 2006). Following this principle, it has been shown that fractional flow responses represent to a diffusion slow-down into fractal networks, and *n* is a function of the fractal dimension and the anomalous diffusion coefficient which likely indicates the presence of connectivity. More recently, Figueiredo et al. (2016) interpreted the sub-radial flow dimension values to be related to the density of channel intersections (or when a fracture is intersected by more than one inflow and one outflow fractures) and local heterogeneities as a function of distance from the pumping well.

The sub-spherical flow regime ($n = 2.5$) also occurs predominantly in our study. By analysing both the lithostratigraphy of wellbore loggings and *n*, we observe that this flow regime is statistically correlated with fractured rocks that are supplied by an overlying granular horizon. Obviously, further field data and consistent numerical results are needed to establish any link between this flow dimension and possible leakage effects. However one author, Doe (2002), stated that for a planar conductor (a horizontal and tabular aquifer) generating a radial flow regime, «leakage over

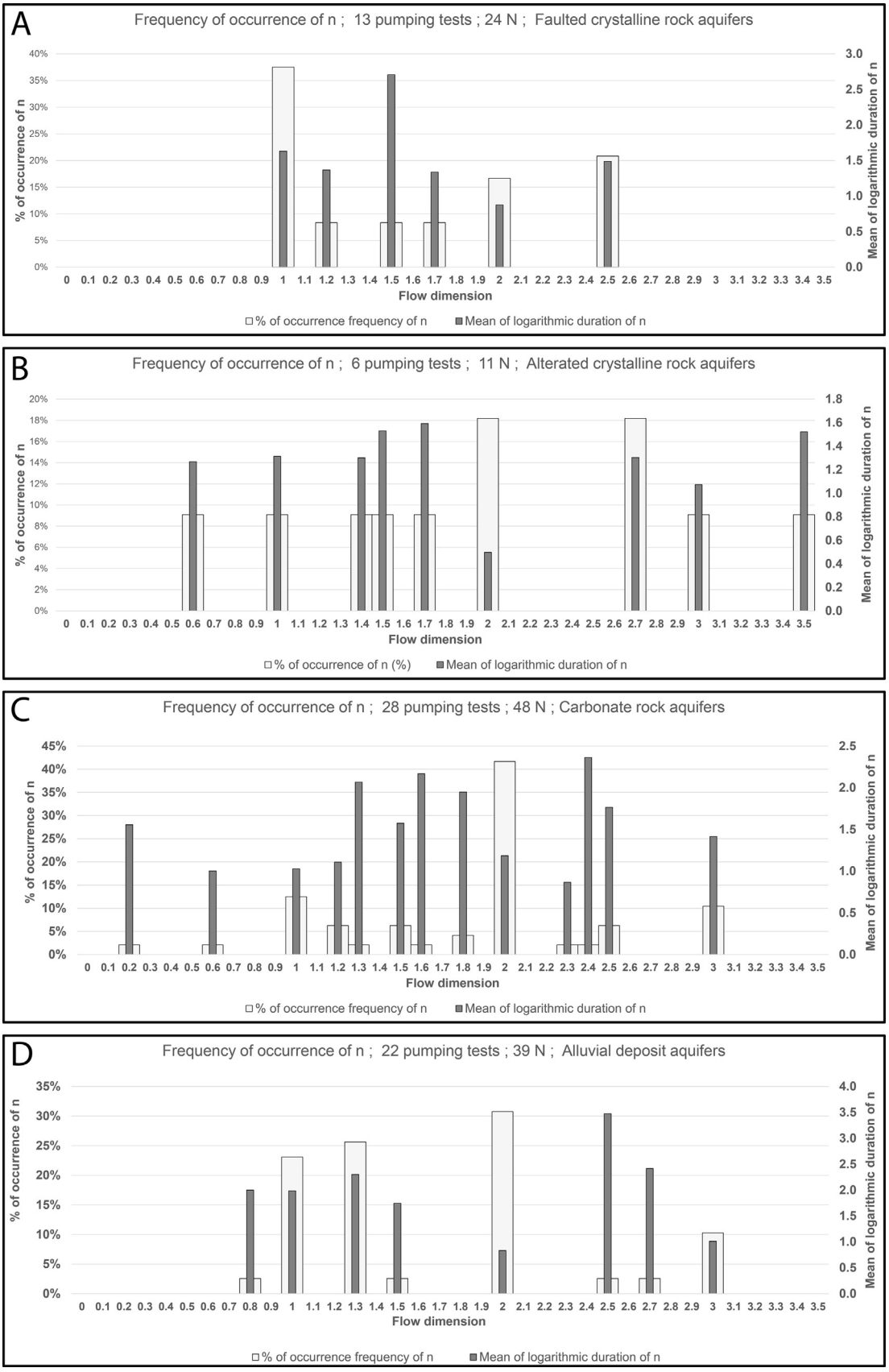

Fig. 10. Statistical analysis of the flow dimension occurrence in 69 constant-rate pumping tests performed A) in altered crystalline rock aquifers, B) in faulted crystalline rock aquifers, C) in carbonate rock aquifers and D) in alluvial deposits. The flow dimension was manually estimated based on a sequential analysis. The large dark bars that represent the flow dimension occurrence are read on the left y-axis. The thin clear bars that represent the mean logarithmic duration of *n* are read on the right y-axis. The "N" in the graph titles represents the number of observed flow dimensions.

the conductor surface may lead to a dimension somewhat greater than 2» (no proof was presented). This phenomenon will be investigated in future works.

Note that 23 % of cases in the FCR group show negative unit slopes of the *ds*/*dlogt* signal, which suggests that there are transitions to higher values of hydraulic properties (Rafini et al., 2017) or transitions to another flow dimension value (Rafini and Larocque, 2012) or transitions to constant-head boundary conditions (Walker and Roberts, 2003). Transitions in FCR aquifers reflect heterogeneity of the fractured media. When constant-head boundary effects are observed in the FCR aquifers, this reflects the existence of hydraulic relationships between the fractured media and lakes or rivers on the surface, or may reflect a significant increase of the hydraulic conductivity or of the storage coefficient (for instance, a system of minor faults intersecting a major fault).

The ACR group, composed of 6 pumping tests and 10 *n* values, is represented by flow dimension values ranging from 0.6 to 3.5 (Fig. 10-B). The spherical and the radial flow dimensions are frequently observed and each represents 18 %, but the radial flow is only observed during a short period of time. The radial flow dimension is observed at early times or at late times, depending on the derivative signatures. The ACR group is composed of sub-linear ($n = 0.8$), linear ($n = 1$), sub-radial ($n = 1.4 - 1.5 - 1.6 - 1.7$), radial ($n = 2$), sub-spherical ($n = 2.7$), spherical ($n = 3$) and hyper-spherical-spherical ($n = 3.5$) flow dimensions. Comparatively to the FCR group, the ACR group demonstrates a lesser proportion of linear flow values and a greater proportion of *n* values higher than 2.7. The spherical flow dimension is observed in the ACR group, whereas it is not observed in the FCR group. These features may be expressions of the effects of chemical alterations on FCR aquifers. Indeed, chemical alteration increases the fracture density and the connectivity between fractures, leading to a thicker flow media in which the pressure front pulse can expand more easily. The altered rock aquifers are characterised by granitic sand overlaying a fractured-weathered layer, requiring the use of a screened borehole. Chemical alteration processes tend to increase the connectivity of existing fractures, leading to an enhancement of the permeability of hard rock aquifers (Lachassagne, 2008; Lachassagne et al., 2011; Worthington et al., 2016). According to these authors, chemical processes such as the swelling of certain minerals can widen fractures. As may be expected, such expansion of the volume and hydraulic activity of fractures is revealed by a statistical increase of the flow dimension, as observed here, as well as a higher occurrence of the spherical flow regime. In this context, the spherical flow regime likely reflects conditions of a partially penetrating well, in other words, a situation in which a full volume aquifer which has a thickness much greater than the screened or open-borehole window (Escobar et al., 2012; Ferroud et al., 2015). This supposes that the density and connectivity of the fracture network are sufficiently high, presumably as a consequence of weathering, for the network to behave like a three-dimensional continuum. Conceptually, the well is associated with a point source involving a cross-flow area expansion in the form of concentric spheres. The value of *n* greater than 3 ($n = 3.5$), which is a long-term and low-noise signal (Fig. 11), is enigmatic and requires more field and numerical investigations in order to be better understood. However, we provide some possible explanations in the general discussion section.

4.2.2.2. Carbonate aquifers. The histogram of carbonate rock aquifers was established based on 29 pumping tests located in the regions of Mirabel, CHCN, SLSJ (Quebec), Nord-Pas-de-Calais, Midi-Pyrénées (France) and Kef (Tunisia). The most observed *n* values are: $n = 2\text{-}1\text{-}3 - 1.2 - 1.5 - 2.5$ representing, respectively, 42 %, 13 %, 10 %, 6 %, 6 % and 6 % of the carbonate group, lasting, respectively, 1.2, 1, 1.4, 1.1, 1.6, 1.8 log cycles (Fig. 10-C).

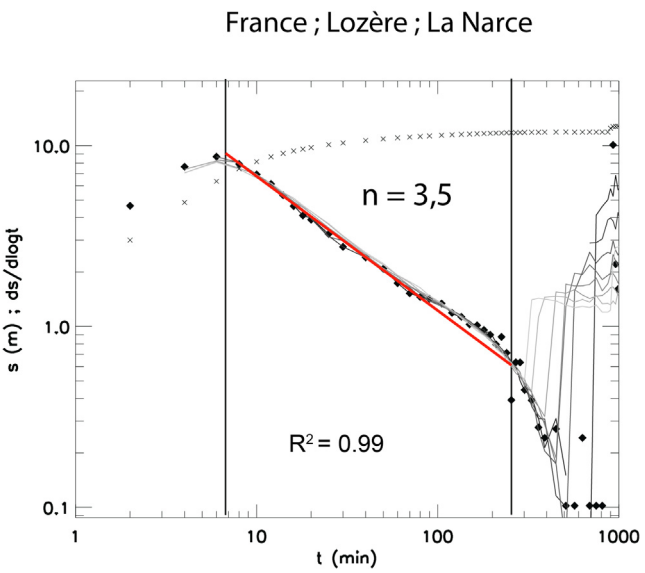

Fig. 11. Example of a diagnostic plot with a flow dimension value greater than 3 ($n = 3.5$). The diamond shapes represent the drawdown log-derivative signal and the "x" shapes represent the drawdown signal. The well test was performed in a weathered crystalline rock located in France. The fit is performed using the SIREN code. The quality of the manual fit is evaluated using the determination coefficient R^2 between the regression line and the derivative data. The $n = 3.5$ is assumed to be induced by a partially penetrating/completed/screened well which is influenced by leakage.

In terms of the ratio between the frequency of occurrence of *n* and its average log-duration, the radial flow regime is the most significant. Rafini and Larocque (2012) demonstrated that a radial flow regime can be generated by horizontal faults. Jourde et al. (2002) stipulated that a radial flow regime can be observed in an orthogonal discontinuity network when the fractures are well-connected. In general, when the pressure front-pulse is large enough, smaller occasional heterogeneities will exert only a negligible impact on the large-scale flow behavior. In such a case, the aquifer would be associated with an equivalent continuous media where a radial flow regime is feasible.

Furthermore, in fractured carbonate rocks, the flow is supposed to be mainly governed by horizontal plane fractures that are cross-connected by vertical fractures (Novakowski and Lapcevic, 1988; Zanini et al., 2000). Such a conceptual model is well-supported by the large proportion of $n = 2$ values reported in these environments. The early-time radial flow observed in our database may indicate that the bedding plane fractures are well-connected and contribute to the flow. Whereas the late-time radial flow may be associated with the continuous-like fracture network contribution at large scale. When the cross-flow area is large enough, the fractured dolomite, which generally presents a well-developed fracture network that is cross-connected to a less-developed bedding plane fracture network, is also favorable to the development of a radial flow dimension. Finally, conceptual models with horizontal planes that exhibit only plane beddings, such as those composed of pure non-fractured limestones, are also favorable to the establishment of a radial flow dimension (Rafini and Larocque, 2012).

Fig. 10-C shows the presence of $n = 1$, implying the influence of a vertical fault or an intersection of faults. The size of the discontinuity may be understood based on the time-period during which the flow regime occurs: an early-time linear regime may be due to a submeter scale vertical fracture, while a late-time linear regime may reveal the presence of large-scale vertical faults. On the contrary, the value of $n = 1.5$ expresses the presence of a

leaky-vertical fault supplied by a conductive matrix embedded in the fracture network, which is sufficiently transmissive and connected in order to significantly feed the fault.

The fractional values of flow dimension (non-integer n values) are commonly interpreted to be associated with the fractal properties of fractured rock systems (crystalline or carbonate aquifers). The fractal flow models assume that the fractured rock is composed of scale-invariant fracture geometries. When during a same pumping test a sequence of integer and non-integer values of n are observed, this compromises the fractal theory which is based on assumptions regarding the homogeneity and density of fractures. The mismatch between the fractal dimension and n has been reported (Verbovšek, 2009; Rafini and Larocque, 2012). Indeed, Verbovšek (2009), using a statistical approach, shows that the fractal dimension parameter (obtained by the classic box-counting method) and n (obtained by an automated type-curve matching of the drawdown log-derivative signal) are not correlated. He interprets the fractional n values as being related to the degree of connectivity between the fractures.

Carbonate rocks are the context with the most variable flow dimension values. The values range between 0.2 and 3 with fractional sub-radial flow dimensions of n = 1.2 – 1.3 – 1.5 – 1.6 – 1.8 and sub-spherical flow dimensions of n = 2.3 – 2.4 – 2.5. This variability in flow dimension reflects an important variability of fracture and fault configurations. As shown by the thin dark bars of Fig. 10-C, these flow dimensions are generally stable and long-term. This variability in the n values reflects environments with a variability of fractures and/or fault configurations.

Some pumping tests performed in carbonate rock aquifers exhibit late times unit slopes. In the petroleum literature, such a flow regime is commonly associated with a reservoir that is depleted with no spatial diffusion of drawdown (among others, Mattar 1997, Ehlig-Economides and Vera, 2013). In other words, the no-flow boundaries have been attained. This assumption is consistent with carbonate systems, where sealing faults are frequent due to self-forming calcite or clay seals. This late time unit slope may express the attainment of sealing faults or impermeable boundaries in every direction. Observing this signal in CFR aquifers suggests either that the productive zones are limited to specific fracture zones in the vicinity of the pumping well, or that sealed faults are frequently reached by the pressure wave.

Negative unit slopes are also observed between some flow dimensions and may reflect a transition period between two flow dimensions or may be related to a significant change in hydraulic conductivity. For instance, the dual-porosity model (Warren and Root, 1963) assumes a transitional flow period between two radial flow regimes which represents, firstly, the water supply from the fracture network and secondly, the water supply from the matrix. Rafini and Larocque (2012) show that when a finite-conductive vertical fault is not connected to the well, a transitional flow period is observed between the radial flow through the matrix and the bilinear flow through the leaky fault. The frequent occurrence of negative unit slopes thus expresses heterogeneous media with participation of several flow regimes.

4.2.2.3. Fluvial-glacial deposit aquifers. The fluvio-glacial-deposit (FGD) histogram generated in this study comprises 22 pumping tests conducted in the regions of CHCN and SLSJ (Quebec) and the eskers of the Abitibi region (Quebec). The most prominent flow dimensions, in terms of frequency of occurrence and duration, are represented by n = 1.3 and 1, representing, respectively, 20 % and 17 % of the FGD group (composed of 46 n values), lasting respectively 2.2–2.3 log-cycles (Fig. 10-D).

All the pumping tests performed in the eskers of the Abitibi region showed a long-term and single-stage pseudo-linear flow regime (n = 1.3). The linear flow regime in fluvioglacial deposits has until now seldom been investigated. Two studies interpreted the linear flow in granular aquifers to be related to two different contexts:

i. a long and narrow system which channels the flow between two parallel impermeable hydraulic boundaries or low-permeability levees (Escobar et al., 2004a; Escobar and Montealegre-M, 2007). Such systems may be observed in channelized deposits such as glacial hollows filled by sediments or eskers.
ii. Micro-cross flow within non-communicating layers. Indeed, by modelling pumping tests in fluvial deposits, Corbett et al. (2012) observed that the deposit systems, formed by the transport and deposition of sediments, exhibit characteristics of hydraulic conductivity distribution, anisotropy and geometry which strongly influence the hydraulic behavior of these systems. They showed that a decrease of lateral transmissivity and a poor lateral connectivity of facies favor the development of an increasing slope of the derivative signal (which implies a linear/pseudo-linear n), which they named the "ramp" effect.

As stated by Corbett et al. (2012), the internal properties of fluvial sediments are valuable assumptions which greatly contribute to the interpretation of such linear flow regimes. Being long and narrow systems, eskers are fluvioglacial deposits whose geometry favors the establishment of linear flow regimes. However, the pseudo-linear flow regimes observed in the database are more enigmatic. More field and numerical studies are needed to determine the geological facies involved in such flow regimes.

A significant number (8 %) of spherical flow regimes are reported in this study, notably in thick deposit aquifers. These systems, characterized by a screen thickness significantly smaller than the aquifer thickness, favor the establishment of n = 3. In some cases, the variable thickness aquifer is a more valuable conceptual model to explain this value of n. For instance, one of the pumping tests, showing a spherical flow, was performed in a topographic depression that had been carved and then filled by glaciers. The geometrical increase of the aquifer thickness associated with the depression favors the establishment of a spherical flow regime (Dal Soglio, 2012; Rafini et al., 2014).

The FGD group displays early unit negative slopes of the *ds*/*dlogt* signal which may indicate a transition period between the wellbore effects and the aquifer's signal (Tiab, 1995). It is not surprising to observe wellbore effects more frequently in deposit aquifers than in fractured aquifers, because granular boreholes require a screen which may induce skin effects, while the borehole dug into fractured rock is a simple open hole without a screen.

As explained above, fractional n values are widely interpreted to reflect the fractal properties of the fractured rock media, an interpretation that is challenged by the observation of frequent non-integer values of n in granular aquifers, mostly in the range of 1–2.

It should be noted that no relationship between n and the confinement conditions of the aquifer (confined/unconfined) has been observed. The typical type-curve provided by Neuman's solution has not been observed either.

5. Discussion

This study has collected and summarized the flow dimension values of several pumping tests and reviewed the current published assumptions used to interpret these flow dimension values. Any flow model where the transient flow area changes by a certain

value of the power of the distance to the well corresponds to a specific flow dimension. This is the reason why the assumptions presented in the "Result and discussion" section are non-unique; it is possible for different hydraulic and geometrical configurations to yield a same value of flow dimension.

When conducting the *n*-sequential analysis, it is important to keep in mind that the propagation of the pressure front-pulse is a diffusive process, and that the drawdown behavior is governed by averaged conditions rather than by local heterogeneities (Horne, 1995). Furthermore, the flow dimension is not an integrative value that would represent a combination of all the flow regimes. Rather, it is an apparent value that reflects the dominant flow regime which influences the cross-flow area diffusion felt by the pressure-front pulse. For instance, as modeled by Rafini and Larocque (2012), a vertical leaky fault located in a homogeneous matrix generates the *n*-sequence 1.5–2, reflecting, firstly, the influence of the fault and secondly, the influence of the matrix. Under no circumstance will the second *n* express a mean value between the two flow regimes. Rather, it should be underlined that the second flow regime is a value that expresses the flow regime related to the most influential flow of the hydrogeological facies. The sequences of *n* can thus be interpreted independently and successively. Because each flow regime observed during a single pumping test exists independent from any other, it is conceivable to interpret an *n*-sequential signal by successively matching various analytical solutions (as done by Hammond and Field, (2014)).

The drawdown log-derivative signal and Barker's law help in better interpreting the flow regime occurring during a constant-rate pumping test. In order to use the flow dimension value as a diagnostic tool, it is important, however, to keep in mind that the cross-flow area is growing as the pressure wave is diffused through the aquifer. Due to the expansion of the cross-flow area, a variation in the observational scale must be considered. Hence, the sensitivity of the transient well test signal to small heterogeneities diminishes as the radius of investigation increases. Beauheim et al. (2004) highlighted the importance of considering the scale when analysing the flow dimensions of pumping tests in a heterogeneous aquifer. They stated that for a single pumping well, different estimated flow dimensions can be obtained, depending on the pumping test method used. Indeed, some of these pumping tests may not have the same radius of investigation, such as for instance slug test compared to pumping test. It is worth noting that the extent and the diffusion rate of the radius of investigation is independent of the pumping rate, because it is an intrinsic value only associated with the diffusive properties of the aquifer (transmissivity and storage).

The interpretation of flow regimes employs successive linear regressions on derivative data, into several time windows. The recognition of these time windows, and the confidence this provides for the interpretation of flow dimension, remains a sensitive aspect of the approach that may, in some cases, leave uncertainties. A manual interpretation is recommended rather than any automated process which optimizes regression coefficient sequences. Indeed, the quality of regressions is not the only component of a proper interpretation of flow regimes: a manual analysis of derivative data makes it possible to identify pumping rate stops or changes, to award a lesser degree of significance to certain noisy sections that have a more obvious and greater degree of data instability – either instrumental, due to a temporary high diffuse heterogeneity field, or for other reasons. Furthermore, the practitioner conducting a manual interpretation may benefit from derivative differentiation without being misled by it, in other words, to "stick to raw data". We finally submit that a simultaneous fit on both *s* and *ds*/*dlogt* significantly contributes to reducing subjectivity issues regarding the interpretation of flow regimes.

A major issue of any derivative analysis remains the quality of the data. Even though derivative data are, advantageously, highly sensitive to hydrodynamic changes in the aquifer, they are also strongly impacted by noise sources, either natural or instrumental. It is not rare that noise impedes any confident and unique interpretation of derivative curves. As stated by Anderson et al., (2006), interpreting a pumping test without taking data quality into account can lead to the erroneous understanding of aquifer features. Various differentiation methods are proposed in the literature to improve the signal/noise ratio. The deconvolution techniques, initially proposed by Birsoy and Summers (1980) in hydrogeology and by von Schroeter et al. (2001) and Azi et al. (2008) in the petroleum industry, make it possible to assess the equivalent constant-rate drawdown of a variable-rate test. The practice is extremely popular in petroleum studies to process the transient tests before their interpretation (Azi et al., 2008; Gringarten, 2010; Onur and Kuchuk, 2012; Obeahon et al., 2014). These approaches require knowledge of the drawdown *s*, the time *t* and the pumping rate *Q*. It may be advantageous to adopt this data processing practice in hydrogeology studies in order to improve the accuracy of interpretations. The deconvolution tools could not have been integrated in this study due to the lack of detailed pumping rate survey data.

Even though variations in pumping rate steps do not influence the estimation of the flow dimension (because single variations do not change the general trend of the derivative signal and may thus be disregarded in the analysis), each pumping rate adjustment strongly affects the derivative signal by generating significant noise. Thus, analysing the recovery data appears to be a favorable option. Practitioners must, however, be aware that drawdown and recovery signals are not necessarily similar. As stated by (Mattar, 1997, 1999), the differences between the drawdown and the buildup data appear when the test is affected by aquifer heterogeneities or boundaries. Because the analytical type curves are mostly configured for drawdown, the drawdown data are needed to estimate the hydraulic properties. The buildup signal should be interpreted qualitatively, in addition to the drawdown data (because it is not subject to disturbances caused by changes in pumping rate). The buildup signal should indeed be analyzed in order to help with the diagnostics rather than for quantitative analysis.

When using the derivative signal in order to estimate the hydraulic properties of the aquifer, it is important to keep in mind that i) the flow dimension value can reflect the geometry of the aquifer and/or the geometry of the well and/or the geometry of the flow and/or the geometry and connectivity of fractures (in fractured media); and ii) certain mechanisms can disrupt the signal of the aquifer. In early times, the signal of the aquifer can be masked or disrupted by wellbore effects. At middle times, the aquifer's signal can be influenced by rain infiltration or leakage. At late times, the signal of the aquifer can be masked by boundary conditions. When interpreting flow regimes, it is therefore important to have good knowledge of the environment surrounding the well and the conditions of the pumping tests. Further numerical simulations are needed to i) distinguish such effects from the aquifer's signal and ii) develop analytical equations for non-radial flow regimes.

The spherical flow dimensions of the entire database were analyzed, in order to correlate the well conditions of a partial penetrating/completed/screened pumping well with the frequency of occurrence of the spherical flow dimension. The spherical flow dimension is observable in 10 pumping tests, four of which were performed in alluvial deposits, two in weathered crystalline rock aquifers, three in carbonate rocks and one with a screen intercepting both a carbonate rock and a moraine (Table 6). According to Escobar et al. (2012), the early-times flow dimension is signifi-

Table 6
Summary of the pumping tests that show a spherical or a hyper-spherical flow dimension (highlighted in bold in the *n*-sequence column) with their intercepted aquifer thickness, their screen thickness and the ratio between both thickness and our interpretation of the spherical flow dimension. In the "location" column, the abbreviations CHCN, SLSJ and Qc designate, respectively, Charlevoix-Haute-Côte-Nord, Saguenay-Lac-Saint-Jean and Quebec. In the "*n*-sequence" column, the abbreviations MG, G and VG represent the appreciation of the quality of the *ds/dlogt* signal and signify, respectively, mediocre-good, good and very good. The letter (U) indicates either an undefinable slope of the *ds/dlogt* signal or a slope that has not been considered as a flow dimension, but rather as a transition or a boundary effect.

Location	Pumping well name	Simplified geology	Confinement condition	*n*-sequence	Intercepted aquifer thickness (m)	Screen thickness (m)	Penetration ratio	Remarks and interpretations of $n = 3$
Baie-Saint-Paul (CHCN, Qc)	P-1	Alluvial deposits	Confined	2 (MG); **3** (VG);	27.3	8	29 %	Partial penetration
Saint Siméon (CHCN, Qc)	P-1	Alluvial deposits	Confined	2 (M); (U); **3** (MG); 2 (MG); 1 (G);	39.32	0.99	3 %	Partial penetration
Saint-Félicien (SLSJ, Qc)	PE-3	Carbonate rocks+ Alluvial deposits	Confined	2 (MG); (U); **3** (G);	10.5	3.05	29 %	Partial penetration
Lozère (France)	LaNarce	Weathered crystalline rocks	N/A	2 (M); **3.5** (VG); (U);	116	18	16 %	Partial penetration + leakage
Longue-Rive (CHCN, Qc)	P-1	Alluvial deposits	Confined	1.3 (M); **3** (VG); 2.7 (MG);	9.75	5.56	57 %	Other conditions
Pays de la Loire (France)	Mout_3	Weathered crystalline rocks	N/A	(U); **3** (VG); (U);	74.36	40	53 %	Other conditions
Mirabel (Qc)	StJanvHamel	Carbonate rocks	N/A	1 (MG); **3** (MG); 1 (MG);	N/A	0	N/A	The pumping well is located in a fracture; $n = 3$ may represent a transition between the two linear flow dimensions.
La Malbaie; Joyeuse (CHCN, Qc)	PP-5D	Alluvial deposits	Unconfined	1 (MG); **3** (G); 2 (MG);(U);	4.04	3.05	75 %	The static level is 0.77 m above the top of the screen
Midi-Pyrenees (France)	Faha	Carbonate rocks	Partially-confined	(U); **3** (MG); 2 (MG);	N/A	30	N/A	Lack of data
Mirabel (Qc)	MT2	Carbonate rocks	N/A	(U); **3** (MG);	N/A	0	N/A	Lack of data

cantly influenced by the penetration ratio of the pumping well. Moncada et al. (2005) explained that the typical −0.5 slope of the *ds*/*dlogt* signal, which is characteristic of the spherical flow dimension, is absent for penetration ratios greater than 40 %. Based on this knowledge, we interpret three pumping tests to be related to partial penetration effects because the penetration ratios are lower than 29 % (Table 6). The pumping well of La Narce shows a long-term and weakly noisy signal with $n = 3.5$ (Fig. 11). We suggest that this hyper-spherical flow dimension may reflect a partial penetrating well effect combined with leakage effects. We will discuss this assumption in the next paragraph. Unfortunately, three pumping tests with $n = 3$ are not interpretable due to a lack of data or poor conditions (the static level is 0.77 m above the top of the screen and the dynamic level is below the top of the screen). Finally, three of the signatures show a spherical flow dimension but cannot be interpreted with the partially penetrating well effects, suggesting that other conditions may produce such a spherical flow dimension. The non-unicity of the derivative signal has already been reported in the literature and will be discussed in the next sections. More field and numerical analyses are thus needed to interpret these pumping tests.

This paragraph aims at providing some thoughts about Barker's model and widening the concepts of the flow dimension parameter that may be related to leakage effects. Since the initial development of the GRF model by Barker (1988), the interpretation of the flow dimension has been extended. As previously explained in Section 2.2.2, the fractal interpretation of fractional values has been open to non-space filling (Doe, 1991), non-fractal fractured media settings (Jourde et al., 1998; Maréchal et al., 2008; Giese et al., 2017) and non-homogeneous systems (Rafini and Larocque, 2009). Rafini and Larocque (2009, 2012) explained that a vertical fault, which is expected to induce a linear flow dimension ($n = 1$), actually produces a bilinear flow dimension ($n = 1.5$), because the flow from the matrix supplies the fault. Furthermore, we observed a statistical correlation between the sub-spherical flow dimension ($n = 2.5$) and the fractured rocks that are supplied by an overlying granular horizon. In addition, Doe (2002) explained that a media inducing a radial flow dimension, which is supplied by leakage, "may lead to a dimension somewhat greater than 2". These observations lead us to suppose that the sub-radial flow dimensions ($2 < n < 3$) may reflect a system that induces a radial flow dimension which is supplied by leakage. Also, we observed a sub-radial flow dimension ($n = 1.3$) in eskers that are highly transmissive flow conduits supplied by surrounding alluvial deposits. In the same line of thought, the esker flow system is expected to induce a linear flow dimension. But leakage around eskers results in increasing linear flow dimension to reach sub-radial flow dimension. Thus, a system supplied by leakage seems to induce a flow dimension somewhat greater than expected. Based on this observation, a point source system or a partially penetrating well (that produces $n = 3$), which is supplied by leakage, may induce a hyper-spherical flow dimension. Indeed, we observe a hyper-spherical flow dimension ($n = 3.5$) in the La Nacre weathered crystalline rock (fourth line of Table 6 and Fig. 11). We assume that this value reflects the signal of a partially penetrating well (expected to induce $n = 3$) that is supplied by leakage. This assumption is in line with the conceptual models of weathered crystalline rock aquifers (Lachassagne, 2008; Lachassagne et al., 2011; Worthington et al., 2016).

6. Conclusion

Based on 69 constant-rate pumping tests, this study presents an overview of the occurrence in nature of the flow dimension parameter in fractured/altered crystalline rock aquifers, carbonate aquifers and fluvio-glacial deposit aquifers. The database is provided in Table 7.

Table 7
Principal data (locations, well names, confinement conditions, simplified lithologies and pumping test durations) and *n*-sequences of the pumping tests in the database. In the fifth column, the letters in brackets refer to an evaluation of the quality of the signal: VG = very good, G = good, MG = mediocre-good, M = mediocre and U = either an undefinable slope of the *ds*/*dlogt* signal or a slope that has not been considered as a flow dimension, but rather as a transition or a boundary effect.

Location	Well name	Confinement conditions	Simplified lithology	Sequence of *n*	Pumping test duration (min)
Mirabel (Quebec)	Lésage	–	Alluvial deposits	6.2 (MG); 1.3 (G); 4 (M);	4100
Longue-Rive (Quebec)	P-1	Confined	Alluvial deposits	1.3 (M); 3 (VG); 2.7 (M);	4320
Longue-Rive (Quebec)	P-2	Confined	Alluvial deposits	3 (MG); 2.7 (G);	4320
Saint-Thomas-Didyme (Quebec)	PU-1	Confined	Alluvial deposits	2 (M); 1.5 (MG); 2 (MG);	4320
Saint Siméon (Quebec)	P-1	Confined	Alluvial deposits	2 (M); 4.7 (VG); 2.5 (MG); 0.8(G);	5490
La Malbaie; Rivière Malbaie (Quebec)	PE-R1	Confined	Alluvial deposits	1.3 (G); 2 (G);	5955
Abtibi-Teminscamingue (Quebec)	PP-2	Confined	Alluvial deposits	1.3 (G);	13105
Baie-Saint-Paul (Quebec)	P-1	Confined (artesian)	Alluvial deposits	1 (G); 3 (VG);	5810
Abtibi-Teminscamingue (Quebec)	PP-4	Unconfined	Alluvial deposits	1.3 (G);	1440
Abtibi-Teminscamingue (Quebec)	PP-6	Unconfined	Alluvial deposits	2 (MG); 0 (G); 1.3 (MG);	1440
La Malbaie; Joyeuse (Quebec)	PP-5D	Unconfined	Alluvial deposits	3 (G); 1.7 (G); 0 (VG);	4320
Desbiens (Quebec)	P-1	Unconfined	Alluvial deposits	2 (G); 0.8 (G);	4320
Desbiens (Quebec)	P-2	Unconfined	Alluvial deposits	2 (M); 1 (G);	4320
La Baie (Quebec)	PW-2004	Unconfined	Alluvial deposits	1 (VG);	4320
Shipshaw (Quebec)	PW-1	Unconfined	Alluvial deposits	1 (VG);	4320
Abtibi-Teminscamingue (Quebec)	PP-1	Unconfined	Alluvial deposits	1.4 (G);	4320
Abtibi-Teminscamingue (Quebec)	PP-3	Unconfined	Alluvial deposits	1.3 (G);	4440
Abtibi-Teminscamingue (Quebec)	1/78	Unconfined	Alluvial deposits	1.3 (G);	5280
Saint-Honoré (Quebec)	PW-1	Unconfined	Alluvial deposits	4 (G); 1 (G);	10142
Saint-Honoré (Quebec)	PW-2	Unconfined	Alluvial deposits	4 (M); 1 (G);	10142
Saint-Honoré (Quebec)	PW-3	Unconfined	Alluvial deposits	4 (G); 1 (G);	10142
Abtibi-Teminscamingue (Quebec)	PS-1	Unconfined	Alluvial deposits	1.3 (MG); 3 (MG); 0.6 (MG);	11520
Mirabel (Quebec)	MT2	–	Carbonates	2 (MG); 2.9 (G);	2880
Nord Pas-de-Calais (France)	Monceau_SD2	–	Carbonates	1 (VG);	2880
Mirabel (Quebec)	StJanvHamel	–	Carbonates	1 (G); 2.8 (G); 1 (G);	4320
Mirabel (Quebec)	GK42	–	Carbonates	0.8 (M); 2.5 (G); 2 (G);	4441
Mirabel (Quebec)	StAnne_G_P-8	–	Carbonates	4 (G); 1.5 (VG); 2 (VG); 0(G);	9372
The Alpes (France)	Fich_23	Confined	Carbonates	1.6 (G); 0.8 (G); 4 (M);	1080
Mirabel (Quebec)	R17	Confined	Carbonates	2 (MG); 0 (MG); 2 (MG);	2880
Mirabel (Quebec)	Bell	Confined	Carbonates	2 (VG);	4080
Mirabel (Quebec)	Demix2	Confined	Carbonates	2 (G); 3.8 (MG); 2 (MG);	4295
La Malbaie; Joyeuse (Quebec)	PP-6R	Confined	Carbonates	1.8 (G); 1 (M);	4320
Mirabel (Quebec)	Chatam	Confined	Carbonates	2.4 (G); 3.5 (G);	4320
Mirabel (Quebec)	Greenalko	Confined	Carbonates	2.3 (G); 2 (G);	4320
Mirabel (Quebec)	Leclerc	Confined	Carbonates	2 (M); 0 (M); 1.6 (G);	4320
Mirabel (Quebec)	StJanv_G_Stja2	Confined	Carbonates	0.6 (G); 4 (MG);	10245
Mirabel (Quebec)	Hamel	Confined	Carbonates	0.5 (G); U ((U));	10259
Nord Pas-de-Calais (France)	StHil_F3	Semi Confined	Carbonates	1.2 (G); 2 (VG);	720
Nord Pas-de-Calais (France)	Lim_PZ6	Semi Confined	Carbonates	3 (VG); 0.8 (VG); 4 (M);	1444
Nord Pas-de-Calais (France)	Maubeuge_FE2	Semi Confined	Carbonates	0 (MG); 4 (MG); 0 (MG);	2520
Midi-Pyrenees (France)	Combes	Semi Confined	Carbonates	2 (MG); 0 (MG);	2620
Midi-Pyrenees (France)	Faha	Semi Confined	Carbonates	0.8 (G); 3 (MG); 2 (MG);	2955
Nord Pas-de-Calais (France)	Bachan	Semi Confined	Carbonates	2.5 (G);	4320
Kef (Tunisie)	Ain_Chaam	Unconfined	Carbonates	2 (G); 5 (M); 2 (G);	240
Mirabel; St Eustache (Quebec)	SE5	Unconfined	Carbonates	0.6 (MG); 3.5 (MG);	333
Nord Pas-de-Calais (France)	Monceau_FE1	Unconfined	Carbonates	1.6 (M); 2.8 (G);	2880
Kef (Tunisie)	Ain_Mizeb	Unconfined	Carbonates	0.8 (M); 4 (G); 2 (G);	4317
Isle-aux-Coudres (Quebec)	PE-1	Unconfined	Carbonates	1.5 (GM);	4320
Mirabel (Quebec)	Mbarette	–	Carbonates + Alluvial deposits	1.5 (MG); 2.5 (G); 1.2 (G);	4320
Mirabel (Quebec)	1_87	Confined	Carbonates + Alluvial deposits	2.5 (G); 0 (MG); 2 (G);	4080
Saint-Félicien (Quebec)	PE-3	Confined	Carbonates + Alluvial deposits	1.7 (G); 2.5 (G);	4345
Pays de la Loire (France)	Mout_3	–	Crystalline rocks	3.2 (VG);	900
Pays de la Loire (France)	Mout_2	–	Crystalline rocks	3 (M); 4 (MG); 1.5 (G);	900
Lozère (France)	LaNarce	–	Crystalline rocks	3.4 (G); 4 (M);	2970
Mirabel (Quebec)	PA-2	–	Crystalline rocks	0.8 (G); 2.5 (G); 1 (G);	4320
Mirabel (Quebec)	Oka1	–	Crystalline rocks	2.5 (MG); 0 (G);	4320
Pays de la Loire (France)	Mout	Confined	Crystalline rocks	2.5 (G); 0.5 (G); 2 (G);	900
La Malbaie; Kane (Quebec)	PK-2R	Confined	Crystalline rocks	0.6 (M); 2.5 (G); 2 (M);	4320
La Malbaie; Kane (Quebec)	PK-3R	Confined	Crystalline rocks	1 (VG); 2 (M); 4.6(VG);	4320
La Malbaie; Kane (Quebec)	PK-8R	Confined	Crystalline rocks	1.2 (G); 4 (G); 1 (MG);	4320
La Malbaie; Saint-Fidèle (Quebec)	PP-3	Confined	Crystalline rocks	2 (G); 1.5 (G);	4320
Les Escoumins (Quebec)	F-5	Confined	Crystalline rocks	1.5 (MG); 2 (VG); 2.7 (G); 4(M);	4320
Saint-Aimé-des-Lacs (Quebec)	F-1R	Confined	Crystalline rocks	1.7 (G); 2.5 (G);	4320
Petit-Saguenay (Quebec)	P-1	Confined	Crystalline rocks	1 (G); 1.7 (G); 2.5 (G);	4320
Ferland-et-Boileau (Quebec)	PP	Confined	Crystalline rocks	1 (G); 1.7 (M);	4435
Saint-Irénée (Quebec)	SI/FE-607	Confined	Crystalline rocks	0 (G); 1.5 (VG); 0 (G);	8601
Pays de la Loire (France)	Beaufou	Confined (artesian)	Crystalline rocks	1.7 (MG); 2.7 (MG); 1 (MG);	21153
La Malbaie; Saint-Fidèle (Quebec)	P-3	Confined	Crystalline rocks	1 (G);	2280
Pays de la Loire (France)	Frapp	Semi-confined	Crystalline rocks	1.4 (G); 2.8 (G);	900
La Malbaie; Joyeuse (Quebec)	PJ-7R + PJ-6R	Unconfined	Crystalline rocks	3 (MG); 1.2 (VG); 2(G);	4320

The real flow dimension statistics obtained in this study emphasize the generally major prevalence of non-radial flow regimes in nature, expressed by a wide diversity of n values. Indeed, the flow dimension values obtained in this study range between 0 and 3.5 with 69 % of the 121 interpreted flow dimensions producing a value for n that is different from 2.

A key element of information obtained in this study is that the flow dimension analysis delivers results that are significantly different from one geological setting to another in terms of n values, variability of the duration of n and n sequences. More particularly, the most statistically significant flow dimensions (in terms of duration and frequency of occurrence) display a higher degree of correlation with the geological conditions around the well. This shows that the hydrodynamic interpretation of these flow dimensions has a physical expression that may relates to the geological framework. This confirms the positive association between conceptual models and flow dimension analysis. For instance, faulted hard-rock aquifers exhibit a high proportion of linear flow regimes, which may express drawdown diffusion through vertical faults embedded into no-flow boundaries, or one-dimensional flow conduits formed by an intersection of faults. Pumping tests performed in altered crystalline rocks and thick alluvial aquifers preferentially produce spherical and pseudo-spherical flow regimes. These can be related to partial completion/penetration of wells or partial screening effects, which produce point sources generating spherical equipotential surfaces or any aquifer's configurations that may lead to a proportional relation of the cross-flow area $A(r)$ and r^2. Fluvio-glacial aquifers exhibit a high frequency of single-stage linear or pseudo-linear responses. These were related to channelized shapes typical of fluvio-glacial environments, such as eskers or micro-cross flows which result from internal heterogeneities within the granular layers. It is interesting to note that, contrary to common opinion, the radial flow assumption is in many cases not suitable to model granular aquifers of the database. Finally, carbonate-rock aquifers exhibit a high proportion of radial flow regimes, interpreted either as the influence of conductive horizontal strata or of large-scale equivalent continuous media.

The use of derivative data allows for a much greater degree of uniqueness of the interpretative type-curves as compared to drawdown-only. Observing similar flow dimensions in different geological facies raises the issue of non-uniqueness of the log-derivative signal. For instance, linear flow regimes have been observed in both fractured rock and fluvio-glacial-deposit aquifers. As stated by Mattar (1997), several conceptual models predict identical *ds*/*dlogt* type-curves, but the estimated aquifer parameters (geometry, hydraulic properties) will be very different from one model to the other. Massonnat and Bandiziol (1991) and Liang et al. (2012) point out the critical insights regarding the geological context to take into account when choosing the adequate analytical model. An interesting continuity of this paper would be to review all the sequences of n that are observed in nature and analytically modeled, in order to assess the potential advantages of using the n-sequential approach to improve the uniqueness of *ds*/*dlogt* interpretations.

Finally, our compilation revealed that in natural aquifers, radial flow regimes occur quite infrequently, representing, overall, 31 % of the flow regimes that were interpreted for this study. Most of the radial flow dimensions were generally observed at early times and were mostly related to a short and noisy signal. In view of these results, it is remarkable that most interpretative models available in the literature describe various types of combined or modified but still radial behaviors, within the radial interpretative framework. This demonstrates that current and common interpretations, using either Theis or Theis-derived models, are in fact hydraulic approximations as they do not account for the real dimension of flow in aquifers. This calls in question the reliability of any interpretative model that does not integrate a flow dimension analysis. New knowledge about occurrences of n in nature may provide impetus to the development of new non-radial flow conceptual models more representative of observed real situations and, more globally, to further research on the flow dimension parameter. The analysis and interpretation of aquifers based on the results of pumping tests might in fact be in its infancy.

A common, yet non-consensual, conceptual interpretation of fractional flow dimension consists in relating it to a gain or a loss of connections in fractures networks with increasing investigation scale (*e.g.* Leveinen, 2000). However, our compilation of n-values occurrences in various geological contexts indicate that such fractional flow dimensions do not occur more likely in hard-rock than in granular settings (Fig. 10). This leads to consider other avenues than fractured networks for the conceptual interpretation of fractional flow regimes. Furthermore, the database highlighted correlations between some fractional n values and leakage. In fact, some sub-radial (*e.g.* $n = 1.3$), sub-spherical (*e.g.* $n = 2.5$) and hyper-spherical (*e.g.* $n = 3.5$) flow dimensions seem to be related to conceptual models, which are influenced by leakage and which were expected to produce respectively, a linear, a radial and a spherical flow dimension. It has already been established that a vertical fault (expected to induce a linear flow dimension) which is supplied by the matrix produces a bilinear flow dimension ($n = 1.5$) (Rafini and Larocque, 2009). We planned to numerically investigate the issue of leakage in order to confirm our assumptions based on field observations.

From a more practical viewpoint, we now know with more certainty that automatically assuming that a flow regime is radial may lead practitioners to over- or under-estimate the hydraulic properties of the aquifers they are studying. Non-radial flow regimes will typically generate investigation areas whose shape is different from that of a regular circle produced by a cylindrical-radial flow. Consequently, in most real-life cases, WHPA delineation may be significantly biased because of erroneous postulates regarding flow dimension regimes. When a radial flow is observable on a log-log plot of *ds*/*dlogt*, the hydraulic conductivity of the aquifer is accurately estimated when using the radial derivative analysis (Eq. (14)). Aquifer evaluation may be improved by analysing the duration and sequences of the flow dimension as it directly relates to the geometrical diffusion of the pressure front-pulse. Further research work is needed in order to develop equations that estimate the hydraulic properties of a non-radial flow regime aquifer and to better understand the physical meaning of fractional flow dimensions. Finally, we recommend improving hydrogeological pumping test practices through the inclusion of the flow dimension analysis in the pumping test interpretation. In particular, both the head and the pumping rate should be accurately measured using a logarithmic time step. It should be remembered that the derivative signal is very sensitive to small variations of the drawdown and the pumping rate. Pumping rate adjustments will generate noise in the derivative signal and pumping rate drifts can induce an apparent flow dimension, which is different from the equivalent constant-rate flow dimension.

Acknowledgments

The authors acknowledge the financial support of the Natural Sciences and Engineering Research Council (NSERC – federal funding – Canada – Discovery Grants Program) of Canada in the framework of the Individual Discovery Grant Program as well as the "Fonds de Recherche du Québec Nature et Technologies (FRQNT – provincial funding – Quebec (Canada) – New university researchers start up program)" in the framework of the individual grant "Nouveaux-chercheurs" held by Prof. Romain Chesnaux. Ms. Josée Kaufmann is thanked for editorial collaboration. Data were

supplied by Geological Survey of Canada (GSC), the French Board of Geological and Mining Research (BRGM) and the Ministry of the environment of Quebec (MDDELCC). We also thank the anonymous reviewers and Dr. Doe for their valuable comments that have greatly improved the quality of this manuscript.

References

Abbaszadeh, M., Cinco-Ley, H., 1995. Pressure-transient behavior in a reservoir with a finite-conductivity fault. SPE Form Eval. 10, 26–32. https://doi.org/10.2118/24704-PA.

Acuna, J.A., Yortsos, Y.C., 1995. Application of fractal geometry to the study of networks of fractures and their pressure transient. Water Resour. Res. 31, 527–540. https://doi.org/10.1029/94WR02260.

Anderson, D., Scotts, G.W., Mattar, L., et al., 2006. Production Data Analysis–Challenges, Pitfalls, Diagnostics. Society of Petroleum Engineers.

Audouin, O., Bodin, J., 2008. Cross-borehole slug test analysis in a fractured limestone aquifer. J. Hydrol. 348, 510–523. https://doi.org/10.1016/j.jhydrol.2007.10.021.

Azi, A.C., Gbo, A., Whittle, T., Gringarten, A.C., 2008. Evaluation of confidence intervals in well test interpretation results. In: Society of Petroleum Engineers paper No. 113888, Europec/EAGE Conference and Exhibition, 9-12 June 2008, Rome, Italy.

Bangoy, L.M., Bidaux, P., Drogue, C., et al., 1992. A new method of characterizing fissured media by pumping tests with observation wells. J. Hydrol. 138, 77–88. https://doi.org/10.1016/0022-1694(92)90156-P.

Barker, J., 2007. Diffusion in Hydrogeology. Diffus. Fundam. 6, 50.1–50.18.

Barker, J.A., 1988. A generalized radial flow model for hydraulic tests in fractured rock. Water Resour. Res. 24, 1796–1804. https://doi.org/10.1029/WR024i010p01796.

Barlow, J.R.B., Coupe, R.H., 2012. Groundwater and surface-water exchange and resulting nitrate dynamics in the Bogue Phalia basin in northwestern Mississippi. J. Environ. Qual. 41, 155–169. https://doi.org/10.2134/jeq2011.0087.

Barry, F., Ophori, D., Hoffman, J., Canace, R., 2009. Groundwater flow and capture zone analysis of the Central Passaic River Basin, New Jersey. Environ. Geol. 56, 1593–1603. https://doi.org/10.1007/s00254-008-1257-5.

Bear, J., Jacobs, M., 1965. On the movement of water bodies injected into aquifers. J. Hydrol. 3, 37–57. https://doi.org/10.1016/0022-1694(65)90065-X.

Beauheim, R.L., Roberts, R.M., 1998. Flow-dimension analysis of hydraulic tests to characterize water-conducting features. In: Water-conducting Features in Radionuclide Migration, GEOTRAP Project Workshop Proceedings, Barcelona, Spain, June 10-12, 1998. Paris, France: OECD NEA. 287-294. ISBN 92-64-17124-X.

Beauheim, R.L., Roberts, R.M., 2002. Hydrology and hydraulic properties of a bedded evaporite formation. J. Hydrol. 259, 66–88. https://doi.org/10.1016/S0022-1694(01)00586-8.

Beauheim, R.L., Roberts, R.M., Avis, J.D., 2004. Well testing in fractured media: flow dimensions and diagnostic plots. J. Hydraul. Res. 42, 69–76. https://doi.org/10.1080/00221680409500049.

Bhatt, K., 1993. Uncertainty in wellhead protection area delineation due to uncertainty in aquifer parameter values. J. Hydrol. 149, 1–8. https://doi.org/10.1016/0022-1694(93)90095-Q.

Birsoy, Y.K., Summers, W.K., 1980. Determination of aquifer parameters from step tests and intermittent pumping data. Ground Water 18, 137–146. https://doi.org/10.1111/j.1745-6584.1980.tb03382.x.

Black, J.H., 1994. Hydrogeology of fractured rocks – a question of uncertainty about geometry. Appl. Hydrogeol. 2, 56–70. https://doi.org/10.1007/s100400050049.

Bourdet, D., Ayoub, J.A., Pirard, Y.M., 1989. Use of pressure derivative in well test interpretation. SPE Form Eval. 4, 293–302. https://doi.org/10.2118/12777-PA.

Bourdet, D., Whittle, T., Douglas, A., Picard, Y., 1983. A new set of types curves simplifies well test analysis. World Oil 196, 95–106.

Bowman, D.O., Roberts, R.M., Holt, R.M., 2012. Generalized radial flow in synthetic flow systems. Groundwater 51, 768–774. https://doi.org/10.1111/j.1745-6584.2012.01014.x.

Carrera, J., 1993. An overview of uncertainties in modelling groundwater solute transport. J. Contam. Hydrol. 13, 23–48. https://doi.org/10.1016/0169-7722(93)90049-X.

Cello, P.A., Walker, D.D., Valocchi, A.J., Loftis, B., 2009. Flow dimension and anomalous diffusion of aquifer tests in fracture networks. Vadose Zone J. 8, 258–268. https://doi.org/10.2136/vzj2008.0040.

Chang, J., Yortsos, Y.C., 1990. Pressure-transient analysis of fractal reservoirs. SPE Form Eval. 5, 31–38. https://doi.org/10.2118/18170-PA.

Chesnaux, R., Lambert, M., Walter, J., et al., 2011. Building a geodatabase for mapping hydrogeological features and 3D modeling of groundwater systems: application to the Saguenay–Lac-St.-Jean region, Canada. Comput. Geosci. 37, 1870–1882. https://doi.org/10.1016/j.cageo.2011.04.013.

Cinco-Ley, H., Samaniego, V.F., Dominguez, A.N., 1978. Transient pressure behavior for a well with a finite-conductivity vertical fracture. Soc. Pet. Eng. J. 18, 253–264. https://doi.org/10.2118/6014-PA.

Cinco-Ley, H., Samaniego-V. F., 1981. Transient pressure analysis: finite conductivity fracture case versus damaged fracture case. In: SPE Annual Technical Conference and Exhibition, 4-7 October, 1981, San Antonio, Texas, USA, SPE-10179-MS.

Cooper Jr, H.H., Jacob, C.E., 1946. A generalized graphical method for evaluating formation constants and summarizing well-field history. Trans. Am. Geophys. Union 27, 526–534. https://doi.org/10.1029/TR027i004p00526.

Corbett, P.W.M., Hamdi, H., Gurav, H., 2012. Layered fluvial reservoirs with internal fluid cross flow: a well-connected family of well test pressure transient responses. Pet. Geosci. 18, 219–229. https://doi.org/10.1144/1354-079311-008.

Culham, W.E., 1974. Pressure buildup equations for spherical flow regime problems. Soc. Pet. Eng. J. 14, 545–555. https://doi.org/10.2118/4053-PA.

Dal Soglio, L., 2012. Simulation numérique d'essai de pompage pour le diagnostic des discontinuités structurales et des hétérogénéités des aquifères de dépôts.

de Dreuzy, J.-R., Davy, P., Bour, O., 2000. Percolation parameter and percolation-threshold estimates for three-dimensional random ellipses with widely scattered distributions of eccentricity and size. Phys. Rev. E 62, 5948–5952. https://doi.org/10.1103/PhysRevE.62.5948.

Dewandel, B., Lachassagne, P., Zaidi, F.K., Chandra, S., 2011. A conceptual hydrodynamic model of a geological discontinuity in hard rock aquifers: Example of a quartz reef in granitic terrain in South India. J. Hydrol. 405, 474–487. https://doi.org/10.1016/j.jhydrol.2011.05.050.

Doe, T., 2002. Generalized dimension analysis of build-up and pressure interference tests. Stockholm Suède.

Doe, T.W., 1991. Fractional dimension analysis of constant-pressure well tests. In: Society of Petroleum Engineers paper No. 22702, SPE Annual Technical Conference and Exhibition, 6-9 October, 1991, Dallas, Texas, USA. pp 461–467.

Doughty, C., Karasaki, K., 2002. Flow and transport in hierarchically fractured rock. J. Hydrol. 263, 1–22. https://doi.org/10.1016/S0022-1694(02)00032-X.

Ehlig-Economides, C., 1988. Use of the pressure derivative for diagnosing pressure-transient behavior. J. Pet. Technol. 40, 1280–1282. https://doi.org/10.2118/18594-PA.

Ehlig-Economides, C.A., Vera, F.E., 2013. Diagnosing pressure-dependent-permeability in long-term shale gas pressure and production transient analysis. In: Society of Petroleum Engineers paper No. 168698, Unconventional Resources Technology Conference, 12-14 August, Denver, Colorado, USA. Society of Exploration Geophysicists, American Association of Petroleum Geologists, Society of Petroleum Engineers, pp. 569–578.

Escobar, F., Montealegre-M, M., 2007. A complementary conventional analysis for channelized reservoirs. CTF – Cienc. Tecnol. Futuro 3, 137–146.

Escobar, F., Saavedra, N., Hernandez, C., et al., 2004a. Pressure and Pressure Derivative Analysis for Linear Homogeneous Reservoirs Without Using Type-Curve Matching. Society of Petroleum Engineers.

Escobar, F.-H., Corredor, C.-M., Gomez, B.-E., et al., 2012. Pressure and pressure derivative analysis for slanted and partially penetrating wells. Asian Res. Publ. Netw. ARPN 7, 932–938.

Escobar, F.H., Hernández, D.P., Saavedra, J.A., 2010. Pressure and pressure derivative analysis for long naturally fractured reservoirs using the TDS technique. DYNA 77, 102–114.

Escobar, F.H., Hernández, Y.A., Hernández, C.M., 2007. Pressure transient analysis for long homogeneous reservoirs using TDS technique. J. Pet. Sci. Eng. 58, 68–82. https://doi.org/10.1016/j.petrol.2006.11.010.

Escobar, F.-H., Muñoz, O., Sepúlveda, J., Montealegre, M., 2005. New finding on pressure response in long, narrow reservoirs. CTF – Cienc. Tecnol. Futuro 3, 151–160.

Escobar, F.H., Navarrete, J.M., Losada, H.D., 2004b. Evaluation of Pressure Derivative Algorithms for Well-Test Analysis. Society of Petroleum Engineers.

Fadlelmawla, A.A., Dawoud, M.A., 2006. An approach for delineating drinking water wellhead protection areas at the Nile Delta, Egypt. J. Environ. Manage. 79, 140–149. https://doi.org/10.1016/j.jenvman.2005.06.001.

Ferris, J., 1949. Ground Water. In: Hydrology. John Wiley & Sons Inc, New York, United-States, pp. 198–272.

Ferroud, A., Chesnaux, R., Rafini, S., 2015. Pumping test diagnostic plots for the investigation of flow patterns in complex aquifers: numerical results. In: 42nd IAH International Congress "Hydrogeology: Back to the future", September 13-18, 2015, Rome, Italy.

Figueiredo, B., Tsang, C.-F., Niemi, A., Lindgren, G., 2016. Review: The state-of-art of sparse channel models and their applicability to performance assessment of radioactive waste repositories in fractured crystalline formations. Hydrogeol. J. 1–16. https://doi.org/10.1007/s10040-016-1415-x.

Forster, C.B., Lachmar, T.E., Oliver, D.S., 1997. Comparison of models for delineating wellhead Protection areas in confined to semiconfined aquifers in alluvial basins. Ground Water 35, 689–697. https://doi.org/10.1111/j.1745-6584.1997.tb00135.x.

Geier, J.E., Doe, T.W., Benabderrahman, A., Hassler, L., 1996. Generalized radial flow interpretation of well tests for the site-94 project.

Giese, M., Reimann, T., Liedl, R., et al., 2017. Application of the flow dimension concept for numerical drawdown data analyses in mixed-flow karst systems. Hydrogeol. J. 25, 799–811. https://doi.org/10.1007/s10040-016-1523-7.

Gringarten, A., Witherspoon, P., 1972. A method of analyzing pump test data from fractured aquifers. In: Int. Soc. Rock Mechanics and Int. Ass. Eng. Geol. Stuttgart, pp. 1–9.

Gringarten, A.C., 2010. Practical use of well-test deconvolution. In: Society of Petroleum Engineers paper No. 134534, SPE Annual Technical Conference and Exhibition, 19-22 September, Florence, Italy.

Gringarten, A.C., Ramey, H.J., Raghavan, R., 1975. Applied pressure analysis for fractured wells. J. Pet. Technol. 27, 887–892. https://doi.org/10.2118/5496-PA.

Gringarten, A.C., Ramey, H.J., Raghavan, R., 1974. Unsteady-state pressure distributions created by a well with a single infinite-conductivity vertical fracture. Soc. Pet. Eng. J. 14, 347–360. https://doi.org/10.2118/4051-PA.

Grubb, S., 1993. Analytical model for estimation of steady-state capture zones of pumping wells in confined and unconfined aquifers. Ground Water 31, 27–32. https://doi.org/10.1111/j.1745-6584.1993.tb00824.x.
Hamm, S., 1995. Hydraulic characteristics of fractured aquifers in South Korea applying fractal models. Jour. Geol. Soc. Korea 4, 467.
Hammond, P.A., Field, M.S., 2014. A reinterpretation of historic aquifer tests of two hydraulically fractured wells by application of inverse analysis, derivative analysis, and diagnostic plots. J. Water Resour. Prot. 06, 481–506. https://doi.org/10.4236/jwarp.2014.65048.
Hantush, M.S., 1956. Analysis of data from pumping tests in leaky aquifers. Trans. Am. Geophys. Union 37, 702. https://doi.org/10.1029/TR037i006p00702.
Hantush, M.S., 1960. Modification of the theory of leaky aquifers. J. Geophys. Res. 65, 3713–3725. https://doi.org/10.1029/JZ065i011p03713.
Horne RN (1995) Modern well test analysis: a computer-aided approach. Petroway.
Jourde, H., Bidaux, P., Pistre, S., 1998. Fluid flow modelling in orthogonal fracture networks: influence of pumping well location on the hydrodynamic response of the modelled aquifer. Bull. Soc. Geol. Fr. 169, 635–644.
Jourde, H., Cornaton, F., Pistre, S., Bidaux, P., 2002a. Flow behavior in a dual fracture network. J. Hydrol. 266, 99–119. https://doi.org/10.1016/S0022-1694(02)00120-8.
Jourde, H., Pistre, S., Perrochet, P., Drogue, C., 2002b. Origin of fractional flow dimension to a partially penetrating well in stratified fractured reservoirs. New results based on the study of synthetic fracture networks. Adv. Water Resour. 25, 371–387. https://doi.org/10.1016/S0309-1708(02)00010-6.
Kruseman, G.P., Ridder, N.A. de, 1994. Analysis and evaluation of pumping test data, 2. ed. (compl. rev.), repr. International Institute for Land Reclamation and Improvement, Wageningen.
Kuusela-Lahtinen, A., Niemi, A., Luukkonen, A., 2003. Flow dimension as an indicator of hydraulic behavior in site characterization of fractured rock. Ground Water 41, 333–341. https://doi.org/10.1111/j.1745-6584.2003.tb02602.x.
Lachassagne, P., 2008. Overview of the hydrogeology of hard rock aquifers: applications for their survey, management, modelling and protection. In: Ahmed, S., Jayakumar, R., Salih, A. (Eds.), Groundwater Dynamics in Hard Rock Aquifers. Springer, Netherlands, pp. 40–63.
Lachassagne, P., Wyns, R., Dewandel, B., 2011. The fracture permeability of Hard Rock Aquifers is due neither to tectonics, nor to unloading, but to weathering processes. Terra Nova 23, 145–161. https://doi.org/10.1111/j.1365-3121.2011.00998.x.
Le Borgne, T., Bour, O., de Dreuzy, J.R., et al., 2004. Equivalent mean flow models for fractured aquifers: Insights from a pumping tests scaling interpretation. Water Resour. Res. 40, W03512. https://doi.org/10.1029/2003WR002436.
Lemieux, Y., Tremblay, A., Lavoie, D., 2003. Structural analysis of supracrustal faults in the Charlevoix area, Quebec: relation to impact cratering and the St-Laurent fault system. Can. J. Earth Sci. 40, 221–235.
Lemieux, J.-M., Therrien, R., Kirkwood, D., 2006. Small scale study of groundwater flow in a fractured carbonate-rock aquifer at the St-Eustache quarry, Québec, Canada. Hydrogeol. J. 14, 603–612. https://doi.org/10.1007/s10040-005-0457-2.
Levasseur, D., 1995. Les eskers : essai de synthèse bibliographique.
Leveinen, J., 2000. Composite model with fractional flow dimensions for well test analysis in fractured rocks. J. Hydrol. 234, 116–141. https://doi.org/10.1016/S0022-1694(00)00254-7.
Leveinen, J., Rönkä, E., Tikkanen, J., Karro, E., 1998. Fractional flow dimensions and hydraulic properties of a fracture-zone aquifer, Leppavirta, Finland. Hydrogeol. J. 6, 327–340. https://doi.org/10.1007/s100400050156.
Liang, H., Lin, S., Huang, T., et al., 2012. Identifying the flow dimension in fractured rock using an interference test. J. Pet. Gas Eng. 3, 114–123.
Lods, G., Gouze, P., 2004. WTFM, software for well test analysis in fractured media combining fractional flow with double porosity and leakance approaches. Comput. Geosci. 30, 937–947. https://doi.org/10.1016/j.cageo.2004.06.003.
Maréchal, J.C., Dewandel, B., Subrahmanyam, K., 2004. Use of hydraulic tests at different scales to characterize fracture network properties in the weathered-fractured layer of a hard rock aquifer. Water Resour. Res. 40, W11508. https://doi.org/10.1029/2004WR003137.
Maréchal, J.-C., Ladouche, B., Dörfliger, N., Lachassagne, P., 2008. Interpretation of pumping tests in a mixed flow karst system. Water Resour. Res. 44, W05401. https://doi.org/10.1029/2007WR006288.
Massonnat, G.J., Bandiziol, D., 1991. Interdependence between Geology and Well Test Interpretation. Society of Petroleum Engineers.
Mattar, L., 1997. Derivative Analysis Without Type Curves. Society of Petroleum Engineers.
Mattar, L., 1999. Derivative analysis without type curves. J. Can. Pet. Technol. https://doi.org/10.2118/99-13-63.
Meier, P.M., Carrera, J., Sánchez-Vila, X., 1998. An evaluation of Jacob's method for the interpretation of pumping tests in heterogeneous formations. Water Resour. Res. 34, 1011–1025. https://doi.org/10.1029/98WR00008.
Moncada, K., Tiab, D., Escobar, F.-H., et al., 2005. Determination of vertical and horizontal permeabilities for vertical oil and gas wells with partial completion and partial penetration using pressure and pressure derivative plots without type-curve matching. CTF – Cienc. Tecnol. Futuro 3, 77–94.
Nadeau, S., Rosa, E., Cloutier, V., et al., 2015. A GIS-based approach for supporting groundwater protection in eskers: application to sand and gravel extraction activities in Abitibi-Témiscamingue, Quebec, Canada. J. Hydrol. Reg. Stud. 4 (Part B), 535–549. https://doi.org/10.1016/j.ejrh.2015.05.015.
Nastev, M., Savard, M.M., Lapcevic, P., et al., 2004. Hydraulic properties and scale effects investigation in regional rock aquifers, south-western Quebec, Canada. Hydrogeol. J. 12, 257–269. https://doi.org/10.1007/s10040-004-0340-6.
Neuman, S.P., Witherspoon, P.A., 1969. Theory of flow in a confined two aquifer system. Water Resour. Res. 5, 803–816. https://doi.org/10.1029/WR005i004p00803.
Novakowski, K.S., Lapcevic, P.A., 1988. Regional hydrogeology of the Silurian and Ordovician sedimentary rock underlying Niagara Falls, Ontario, Canada. J. Hydrol. 104, 211–236. https://doi.org/10.1016/0022-1694(88)90166-7.
Obeahon, P.P., Sedgwick, A., Okereke, O., 2014. Practical application of multi rate deconvolution. In: Society of Petroleum Engineers paper No. 172446, SPE Nigeria Annual International Conference and Exhibition, 5-7 August, Lagos, Nigeria.
Odling, N.E., West, L.J., Hartmann, S., Kilpatrick, A., 2013. Fractional flow in fractured chalk; a flow and tracer test revisited. J. Contam. Hydrol. 147, 96–111. https://doi.org/10.1016/j.jconhyd.2013.02.003.
Onur, M., Kuchuk, F., 2012. A new deconvolution technique based on pressure-derivative data for pressure-transient-test interpretation. SPE J. https://doi.org/10.2118/134315-PA.
Paradis, D., Martel, R., Karanta, G., et al., 2007. Comparative study of methods for WHPA delineation. Ground Water 45, 158–167. https://doi.org/10.1111/j.1745-6584.2006.00271.x.
Pechstein, A., Attinger, S., Krieg, R., Copty, N.K., 2016. Estimating transmissivity from single-well pumping tests in heterogeneous aquifers. Water Resour. Res. 52, 495–510. https://doi.org/10.1002/2015WR017845.
Polek, J., Karasaki, K., Long, J.C.S., Barker, J., 1989. Flow to wells in fractured rock with fractal structure. In: Fractal Aspects of Materials, Materials Research Society.
Rafini, S., 2008. Comportement hydraulique des milieux faillés [The hydraulic behaviour of faulted environments]. PhD, Université du Québec à Montréal.
Rafini, S., 2004. Contrôle structural des écoulements en milieux fractures contribution de l'approche combinée simulation de flux – analyse de la déformation. Université du Québec à Montréal.
Rafini, S., Chesnaux, R., Dal Soglio, L., 2014. A numerical analysis to illustrate the usefulness of drawdown log-derivative diagnostic plots in characterizing the heterogeneity of non-Theis aquifers. In: 2014 GSA Annual Meeting, October 19-22, 2014 Vancouver, British Columbia, Canada.
Rafini, S., Chesnaux, R., Ferroud, A., 2017. A numerical investigation of pumping-test responses from contiguous aquifers. Hydrogeol. J. 3, 877–894. https://doi.org/10.1007/s10040-017-1560-x.
Rafini, S., Larocque, M., 2009. Insights from numerical modeling on the hydrodynamics of non-radial flow in faulted media. Adv. Water Resour. 32, 1170–1179. https://doi.org/10.1016/j.advwatres.2009.03.009.
Rafini, S., Larocque, M., 2012. Numerical modeling of the hydraulic signatures of horizontal and inclined faults. Hydrogeol. J. 20, 337–350. https://doi.org/10.1007/s10040-011-0812-4.
Raghavan, R., 2004. A review of applications to constrain pumping test responses to improve on geological description and uncertainty. Rev. Geophys. 42, RG4001. https://doi.org/10.1029/2003RG000142.
Renard, P., Glenz, D., Mejias, M., 2009. Understanding diagnostic plots for well-test interpretation. Hydrogeol. J. 17, 589–600. https://doi.org/10.1007/s10040-008-0392-0.
Rondot, J., 1989. Géologie de Charlevoix. Série de manuscits bruts. Rapport MB 89-21, Ministère de l'Energie et des Ressources du Québec.
Rozemeijer, J.C., van der Velde, Y., McLaren, R.G., et al., 2010. Integrated modeling of groundwater–surface water interactions in a tile-drained agricultural field: the importance of directly measured flow route contributions. Water Resour. Res. 46, W11537. https://doi.org/10.1029/2010WR009155.
Sánchez-Vila, X., Meier, P.M., Carrera, J., 1999. Pumping tests in heterogeneous aquifers: an analytical study of what can be obtained from their interpretation using Jacob's Method. Water Resour. Res. 35, 943–952. https://doi.org/10.1029/1999WR900007.
Theis, C.V., 1935. The relation between the lowering of the piezometric surface and the rate and duration of discharge of a well using ground-water storage. Trans. Am. Geophys. Union 16, 519–524. https://doi.org/10.1029/TR016i002p00519.
Therrien, R., McLaren, R., Sudicky, E., Panday, S., 2010. HydroGeoSphere, A three-dimensional numerical model describing fully integrated subsurface and surface flow and solute transport. DRAFT, Univ. of Waterloo, Waterloo, Ont., Canada.
Tiab, D., 1993. Analysis of Pressure and Pressure Derivatives without Type-curve Matching – I. Skin and Wellbore Storage. Society of Petroleum Engineers.
Tiab, D., 1994. Analysis of pressure and pressure derivative without type-curve matching: vertically fractured wells in closed systems. J. Pet. Sci. Eng. 11, 323–333. https://doi.org/10.1016/0920-4105(94)90050-7.
Tiab, D., 1995. Analysis of pressure and pressure derivative without type-curve matching – skin and wellbore storage. J. Pet. Sci. Eng. 12, 171–181. https://doi.org/10.1016/0920-4105(94)00040-B.
Tiab, D., 2005. Analysis of pressure derivative data of hydraulically fractured wells by the Tiab's Direct Synthesis technique. J. Pet. Sci. Eng. 49, 1–21. https://doi.org/10.1016/j.petrol.2005.07.001.
Todd, D.K., 1980. Groundwater Hydrology. JWiley, New York, Toronto.
Tsang, C.-F., Neretnieks, I., 1998. Flow channeling in heterogeneous fractured rocks. Rev. Geophys. 36, 275–298. https://doi.org/10.1029/97RG03319.
Verbovšek, T., 2009. Influences of aquifer properties on flow dimensions in dolomites. Ground Water 47, 660–668. https://doi.org/10.1111/j.1745-6584.2009.00577.x.

Verbovšek, T., 2011. Hydrogeology and geochemistry of fractured dolomites–a case study of Slovenia. In: Aquifers: Formation, Transport, and Pollution. Nova Science Publishers, Hauppauge, N.Y., pp. 87–147.

von Schroeter, T., Hollaender, F., Gringarten, A.C., 2001. Deconvolution of well test data as a nonlinear total least squares problem. In: Society of Petroleum Engineers paper No. 71574, SPE Annual Technical Conference and Exhibition, 30 September-3 October, 2001, New Orleans, Louisiana, USA.

Walker, D.D., Cello, P.A., Valocchi, A.J., Loftis, B., 2006. Flow dimensions corresponding to stochastic models of heterogeneous transmissivity. Geophys. Res. Lett. 33, L07407. https://doi.org/10.1029/2006GL025695.

Walker, D.D., Roberts, R.M., 2003. Flow dimensions corresponding to hydrogeologic conditions. Water Resour. Res. 39, 1349.

Warren, J.E., Root, P.J., 1963. The behavior of naturally fractured reservoirs. Soc. Pet. Eng. J. 3, 245–255. https://doi.org/10.2118/426-PA.

Winberg, A., 2000. Äspö Hard Rock Laboratory: final report of the first stage of the tracer retention understanding experiments. Svensk kärnbränslehantering AB/Swedish Nuclear Fuel and Waste Management, Stockholm.

Worthington, S.R.H., Davies, G.J., Alexander, E.C., 2016. Enhancement of bedrock permeability by weathering. Earth-Sci. Rev. 160, 188–202. https://doi.org/10.1016/j.earscirev.2016.07.002.

Wyssling, L., 1979. Eine neue formel zur Berechnung der Zuströmungsdauer (Laufzeit) des grundwassers zu einem grundwasser pumpwerk. Eclogae Geol Helvetiae 72, 401–406.

Zanini, L., Novakowski, K.S., Lapcevie, P., et al., 2000. Ground water flow in a fractured carbonate aquifer inferred from combined hydrogeological and geochemical measurements. Ground Water 38, 350–360. https://doi.org/10.1111/j.1745-6584.2000.tb00220.x.